

1 An experimental study of the solubility and speciation of tungsten in

2 NaCl-bearing aqueous solutions at 250, 300, and 350 °C

3
4 Xin-Song Wang ^{a,b*}, Alexander Timofeev ^b, A.E. Williams-Jones ^b, Lin-Bo Shang ^a, Xian-Wu Bi ^{a*}5 *a State Key Laboratory of Ore Deposits Geochemistry, Institute of Geochemistry, Chinese Academy of Sciences, Guiyang*6 *550002, China*7 *b Department of Earth & Planetary Sciences, McGill University, 3450 University Street, Montreal, QC H3A 0E8, Canada*8
9 **Abstract**

10 The solubility of tungsten trioxide solid and the speciation of tungsten in NaCl-bearing solutions have
11 been investigated through experiments conducted at 250, 300, and 350 °C under vapour-saturated
12 water pressure. Based on the results of these experiments, the solubility of tungsten trioxide was
13 controlled by temperature and pH, whereas the NaCl concentration did not affect the solubility except
14 through its influence on the ionic strength of the solution. Two tungsten species were found to be
15 present in the solutions, namely H_2WO_4^0 at low pH and HWO_4^- at higher pH. These two species
16 formed via the reactions $\text{WO}_3 + \text{H}_2\text{O} = \text{H}_2\text{WO}_4^0$ and $\text{WO}_3 + \text{H}_2\text{O} = \text{HWO}_4^- + \text{H}^+$, respectively. The
17 logarithms of the equilibrium constants for these reactions are -5.18 ± 0.26 , -4.97 ± 0.25 , -4.69 ± 0.10 ,
18 and -7.91 ± 0.30 , -7.67 ± 0.29 , -7.52 ± 0.18 for 250, 300, and 350 °C, respectively. In addition, the
19 logarithms of the first and second association constants of H_2WO_4^0 were determined to be 2.72, 2.71,
20 2.83, and 5.59, 6.49, 8.07 for 250, 300, and 350 °C, respectively. These values indicate that H_2WO_4^0 is
21 only important at low pH values (< 2.8), and that HWO_4^- is the dominant tungsten species at pH
22 conditions commonly encountered in nature. The data obtained in this study were used to model the
23 solubility of scheelite and ferberite. This modeling indicates that tungsten concentrations are highest
24 at high temperature in solutions with high salinity, low contents of calcium and iron, and either very
25 low or high pH. The opposite is true for tungsten mineral precipitation from a fluid.

26
27 **Keywords:** Tungsten solubility and speciation; Tungsten mineralization; Hydrothermal systems;

* Corresponding author: wangxinsong@mail.gyig.ac.cn (X.S. Wang); bixianwu@vip.gyig.ac.cn (X.W. Bi)

28 Formation constants.

29

1. INTRODUCTION

30 Numerous studies have shown that economic tungsten deposits (dominantly greisen and quartz-vein
31 type in which scheelite and/or wolframite are the ore minerals) form from NaCl-dominated brines
32 (3~12 wt.% NaCl) at temperatures in the range 200 °C to 400 °C (Campbell and Robinsoncook, 1987;
33 Polyá, 1989; Bailly et al., 2002; Lu et al., 2003; Romer and Lüders, 2006; Wei et al., 2012; Ni et al.,
34 2015; Zhu and Peng, 2015; Lecumberri-Sanchez et al., 2017; Soloviev and Kryazhev, 2017; Korges et
35 al., 2018). Most of these studies have also proposed models for the formation of the ores, e.g., fluid
36 mixing, cooling, boiling, and fluid-rock interaction (Campbell et al., 1984; Polyá, 1988; Bailly et al.,
37 2002; Lu et al., 2003; Ni et al., 2015; Lecumberri-Sanchez et al., 2017; Korges et al., 2018). In order,
38 however, to reliably model tungsten ore formation, the speciation of tungsten at elevated temperature
39 needs to be known, and thermodynamic data are needed for the dominant species. Unfortunately, there
40 is little agreement on the nature of the main tungsten species at elevated temperature and only a small
41 number of studies have reported robust thermodynamic data for aqueous tungsten species based on
42 experiments.

43 Although most researchers consider that tungsten occurs dominantly as tungstate species in
44 hydrothermal fluids and therefore forms ion pairs with cations like H⁺, Na⁺ and K⁺ (Wesolowski et al.,
45 1984; Wood and Vlassopoulous, 1989; Wood, 1992; Wood and Samson, 2000), some researchers have
46 proposed that it also occurs as complexes involving anions, particularly Cl⁻ (Manning and Henderson,
47 1984). Thus, for example, Manning and Henderson (1984) proposed that WCl₆, WOCl₄ or (WO₃)₂Cl₂,
48 are the dominant tungsten species in brines at magmatic conditions. Keppler and Wyllie (1991)
49 reached exactly the opposite conclusion, namely that halogen complexes are not involved in tungsten
50 dissolution at these conditions. Wood and Vlassopoulous (1989) and Wood (1992) evaluated the
51 proposed role of chloride species in the aqueous mobilization of tungsten experimentally by
52 investigating the solubility of WO₃ in HCl-bearing solutions at 500 °C and 300-600 °C, respectively.
53 They showed convincingly that Cl⁻ complexes do not play a role in tungsten transport and, instead,
54 that H₂WO₄⁰ is the dominant tungsten species in HCl-bearing solutions, at least under acidic
55 conditions; they reported equilibrium constants for the corresponding dissolution reaction. In an
56 earlier potentiometric study and temperatures up to 300 °C, Wesolowski et al. (1984) showed that at
57 higher pH, H₂WO₄⁰ gives way to HWO₄⁻ and HWO₄⁻ gives way, in turn, to WO₄²⁻ as the dominant

58 tungsten species. Because of the importance of NaCl-dominated brines in the transport of tungsten in
59 ore-forming hydrothermal systems, some researchers have proposed that the tungstate ion may form
60 stable ion pairs with Na⁺. Indeed, this was the conclusion reached by Wood and Vlassopoulos (1989)
61 from the observation that the solubility of WO₃ increases with increasing NaCl and NaOH contents of
62 aqueous solutions. Because of the lack of a dependence of this solubility on pH, they also concluded
63 that this ion pair is NaHWO₄⁰ and reported an equilibrium constant for the corresponding dissolution
64 reaction. Gibert et al. (1992) re-evaluated the data of Wood and Vlassopoulos (1989) and showed that
65 they could be explained without invoking ion pairs involving Na⁺. Wood and Samson (2000),
66 subsequently argued that, because of the increased electrostatic attraction among ions at high
67 temperature due to the decreased dielectric constant of water, it is highly probable that the neutral ion
68 pair, NaHWO₄⁰, dominates tungsten transport in hydrothermal systems. Recent molecular dynamic
69 simulations for Cu(I), Au(I), and Zn(II) complexes, however, challenge this conclusion by
70 demonstrating that charged species can predominate in high density fluids, even at high temperature
71 (Mei et al., 2014; 2015). In summary, although it has been clearly established that tungstate forms
72 stable species with H⁺, it is not clear whether or not tungstate also forms stable species with Na⁺. In
73 view of this and the importance of NaCl-dominant brines in transporting tungsten in ore-forming
74 systems involving this metal, it is essential that the question of the stability of Na⁺-tungstate ion pairs
75 be resolved, especially for the temperatures of tungsten ore-formation (200 to 400 °C).

76 In this paper, we report results of experiments designed to evaluate tungsten solubility and
77 speciation in the system H₂O-NaCl at temperatures of 250, 300, and 350 °C. These results show that,
78 in solutions containing up to 4 m NaCl (18.9 wt.% NaCl), tungstic acid (H₂WO₄⁰) is the dominant
79 tungsten species at low pH and HWO₄⁻ is the dominant species at mildly acidic to near-neutral
80 conditions. Although the solubility of tungsten (WO₃) increases with increasing NaCl content of the
81 solution, this is due to the resulting increase in the ionic strength of the solution and not the formation
82 of tungstate ion pairs with Na⁺. We close the paper by retrieving thermodynamic data for H₂WO₄⁰ and
83 HWO₄⁻ and using them to model and evaluate mechanisms for the transport of tungsten and the
84 precipitation of scheelite and wolframite in a hydrothermal fluid.

85

86

2. METHODS

2.1. Experiments

87

88 The experimental equipment and methods adopted in this study are the same as those used in previous
89 studies at McGill University (Migdisov and Williams-Jones, 2007; Timofeev et al., 2017). The
90 experiments were carried out in batch-type titanium grade 2 autoclaves, which were heated in a Fisher
91 Isotemp oven equipped with a stainless-steel box to reduce thermal gradients. Prior to each
92 experiment, the autoclaves were cleaned by filling them with 7 wt.% nitric acid (Trace metal grade)
93 for 12 hours, then twice with 3 wt.% ammonia hydroxide (Trace metal grade) for 6 hours, and finally
94 with nano-pure water for 24 hours. This treatment ensured that no tungsten from previous experiments
95 remained on the walls of the autoclaves.

96 The solubility of tungsten (VI) trioxide solid was investigated in aqueous solutions of variable
97 NaCl concentration and pH at temperatures of 250, 300, and 350 °C, and vapor-saturated water
98 pressure. The sodium chloride solutions were prepared to have concentrations ranging from 0.0005
99 mol/L to 4.0 mol/L; the pH of the solutions was varied by adding small amounts of HCl and ranged
100 from 1.12 to 2.97 at ambient temperature. Solid reactant (WO_3 , yellow powder; Alfa Aesar 99.998%
101 purity) was introduced into a small quartz holder (~3.5 cm long) that was then capped by quartz wool
102 to prevent mechanical transfer of the solid to the solution. In order to ensure that the experiments were
103 conducted at conditions for which the tungsten would be in the 6+ state, the oxygen fugacity of the
104 solutions was buffered by MoO_3 (light yellow powder; Alfa Aesar 99.95% purity) and MoO_2 (brown
105 powder; Alfa Aesar, 99% purity), which were introduced into a long, ~11cm, quartz holder. At the
106 beginning of each experiment, the two holders were placed in an autoclave and 14 ml of NaCl-bearing
107 solution was added to it. This solution covered the short holder but not the long holder, the top of
108 which was predicted to be above the level of the liquid during the experiments (Fig.1). Prior to sealing,
109 the autoclaves were purged with nitrogen gas to remove atmospheric oxygen.

110 Kinetic experiments were performed at 250 °C with a 1 mol/L NaCl solution containing 0.01
111 mol/L HCl for durations between 1 and 11 days. The tungsten concentration reached a steady state
112 value after 6 days (Fig. 2). As experiments conducted at higher temperature were predicted to reach
113 steady state concentrations more rapidly, all subsequent experiments were conducted for durations of
114 ≥ 7 days. At the end of each set of experiments, the autoclaves were removed from the oven and
115 quenched to ambient temperature in less than 20 minutes. A 4 ml aliquot of solution was taken from
116 each autoclave for the determination of pH and analysis of chloride concentration. Four ml of 0.5 wt.%
117 optima grade ammonium hydroxide was then added to each autoclave to dissolve any tungsten that

118 had precipitated on the walls during quenching. After an hour, the mixed solution was removed for
119 analysis of its tungsten content. The pH was measured using an accuTupH™ Rugged Bulb
120 Combination pH Electrode purchased from Fisher Scientific. Solutions containing greater than 0.1
121 mol/L Na⁺ were diluted to a concentration less than this prior to measuring their pH. The resulting pH
122 values were corrected to the corresponding pH values for the temperatures of the experiments using
123 HCh software (Shvarov, 2008). Tungsten concentrations were analyzed using Inductively Coupled
124 Plasma Mass Spectrometry after 1250 to 2500 times dilution of the experimental solution using a
125 0.001wt.% optima grade ammonium hydroxide solution. Finally, the WO₃ reactant was analyzed by
126 X-ray diffraction to confirm that new solids had not formed during the experiments and that the
127 measured solubility corresponded only to the dissolution of WO₃; the only phase detected was
128 crystalline WO₃ (Appendix A). X-ray diffraction analysis also confirmed that the buffer solids MoO₂
129 and Mo₂O₃ solid were both present after the experiments.

130 2.2. Data optimization

131 The dissolved tungsten species in the solution were identified from the slope of the logarithm of
132 the molality and activity of tungsten with respect to that of the other ions in each experiment.
133 Thermodynamic properties for these species, including the standard Gibbs free energy and formation
134 constants, were determined from the molality of tungsten, NaCl and HCl in each experiment using the
135 program OptimA (masses corresponding to an excess of the solute, WO₃^{cryst}, and the oxygen buffer
136 assemblage at the end of each experiment were also specified in the input file), which is part of the
137 HCh software package (Shvarov, 2015). The activity coefficient of each ionic species was calculated
138 using the extended Debye-Hückel equation (Helgeson et al., 1981; Oelkers and Helgeson, 1990;
139 Oelkers and Helgeson, 1991):

$$140 \log \gamma_n = -\frac{A \cdot [z_n]^2 \cdot \sqrt{I}}{1 + B \cdot a \cdot \sqrt{I}} + b_\gamma \cdot I + \Gamma \quad (1)$$

141 in which A and B are constants representing Debye-Hückel limiting law parameters (Table 1), b_γ is
142 the extended parameter for NaCl from Helgeson and Kirkham (1974), a is the distance of closest
143 approach, which is specific to the ion of interest, z is the charge of the ion, Γ is a molarity to molality
144 conversion factor, and I is the ionic strength calculated using Equation (2):

$$145 I = \frac{1}{2} \sum_{i=1}^n c_i z_i^2 \quad (2)$$

146 where c_i is the molar concentration of ion i (mol/L) and z_i is the charge of that ion. Parameter I

157 represents the true ionic strength as all the dissolved components were considered. The activity
158 coefficients of neutral species were assumed to be unity. The Haar-Gallagher-Kell and Marshall and
159 Franck models were used to determine the thermodynamic properties and disassociation constant of
160 H₂O for our experimental conditions (Marshall and Franck, 1981; Kestin et al., 1984).

151

152

3. RESULTS

3.1. Identification of the dissolved tungsten species

153 The results of the experiments at 250, 300, and 350 °C are reported in Table 2. In order to determine
154 whether or not tungsten solubility depends on Na⁺ (or Cl⁻) concentration, sets of experiments were
155 conducted with solutions having roughly constant pH (~2) at ambient temperature and variable NaCl
156 concentration. The pH dependency was evaluated with sets of experiments, each of which was
157 conducted with solutions having approximately the same NaCl concentration (the concentrations of
158 the different sets varied from high to low).

160 From Figure 3a, c and e, it is evident that the concentration of tungsten was low and roughly
161 constant at low a_{Na^+} , whereas at higher a_{Na^+} (the Cl⁻ activity is very similar to that of Na⁺) it
162 increased linearly with $\log a_{\text{Na}^+}$. At first glance, these observations suggest that the tungsten species
163 at low Na⁺ (or Cl⁻) activity was H₂WO₄⁰ or HWO₄⁻ or WO₄²⁻, which do not contain Na or Cl, and that
164 at higher Na⁺ (or Cl⁻) activity it was a Na-tungstate ion pair or a tungsten-chloride complex. At low
165 a_{Na^+} , the tungsten concentration was independent of pH (Fig. 3b, 3d, and 3f), which indicates that
166 tungsten solubility was dominated by the neutral tungstate, tungstic acid (H₂WO₄⁰). In contrast, at
167 high Na⁺ (or Cl⁻) concentration, the tungsten concentration increased linearly with pH (the slope
168 varied between 0.77 and 0.95). As previous experiments have shown convincingly that Cl⁻ complexes
169 do not play a role in tungsten dissolution (Wood and Vlassopoulos, 1989; Wood, 1992), the positive
170 correlation of tungsten solubility with pH at high NaCl concentration and also with $\log a_{\text{Na}^+}$, could
171 reflect a major contribution from NaHWO₄⁰ via the reaction:



$$173 \text{Log } K_3 = \text{log } a_{\text{NaHWO}_4^0} - \text{pH} - \text{log } a_{\text{Na}^+}$$

174 An alternative explanation for these correlations is that the increase in WO₃ solubility with
175 increasing $\log a_{\text{Na}^+}$ was due to the increase in the ionic strength of the solution that accompanied the
176 addition of NaCl. In order to test this latter hypothesis, we calculated the total activity of tungsten,

177 assuming that the only tungsten species in solution were HWO_4^- and H_2WO_4^0 . In addition, we
178 normalized all the data for the three experimental temperatures to a pH of 1.8 (350 °C) and 1.4
179 (300 °C and 250 °C), which are the lowest pH values of the experiments at the three temperatures. The
180 normalization was based on the following reactions and equations:



182 $\text{Log } K_4 = \text{log } a\text{HWO}_4^- - \text{pH}$



184 $\text{Log } K_5 = \text{log } a\text{H}_2\text{WO}_4^0$

185 $\text{Log } a\Sigma\text{W (adjusted)} = \text{log}(10^{\text{log } a\text{HWO}_4^- - (\text{pH} - \text{pH}_{\text{Minimum}})} + a\text{H}_2\text{WO}_4^0)$ (6)

186 In Figure 4, we show these normalized data as a plot of $\text{log } a\Sigma\text{W}$ versus pH. From this diagram, it
187 is clear that the logarithm of the adjusted $a\Sigma\text{W}$ is independent of pH. The presence of any NaHWO_4^0 ,
188 in addition to the assumed HWO_4^- and H_2WO_4^0 , would result in a slope greater than 0 in Figure 4 as
189 Reaction 3 is not only pH-dependent but also Na-dependent. The absence of such a slope indicates
190 that NaHWO_4^0 did not contribute significantly to the total dissolved concentration of tungsten in the
191 experimental solutions.

192 As discussed above, NaHWO_4^0 is interpreted not to have been present in the experimental
193 solutions in detectable concentrations, despite the fact that the solubility of $\text{WO}_3^{\text{crystal}}$ increased with
194 increasing NaCl concentration. Instead, we conclude that the solubility data can be satisfactorily
195 explained by HWO_4^- and H_2WO_4^0 . From Figure 5, it can be seen that the tungsten activity was low
196 and constant at low pH and at higher pH increased with increasing pH at each of the temperatures for
197 which the solubility of $\text{WO}_3^{\text{crystal}}$ was determined. The independence of tungsten activity from pH at
198 low values of pH was due to the formation of H_2WO_4^0 according to Reaction 5, which does not
199 involve H^+ . At higher pH values, the increase in tungsten activity with increasing pH was due to the
200 formation of HWO_4^- via Reaction 4, inspection of which reveals that $a\text{HWO}_4^-$ increases with
201 decreasing $a\text{H}^+$ or increasing pH in a ratio of 1:1. This interpretation is supported by the observation
202 that the slope of the dependency of $\text{log } a\text{HWO}_4^-$ on pH ranges between 0.93 and 1.17, depending on
203 the temperature (Fig. 5b, 5d and 5f). The threshold pH above which HWO_4^- replaces H_2WO_4^0 as the
204 dominant species is 2.44 at 350 °C (Fig 5a) and corresponds to a tungsten concentration of ~5.9 ppm.
205 This threshold pH at 300 °C is 2.32, corresponding to a tungsten concentration of ~2.7 ppm and at
206 250 °C is 2.22, corresponding to a tungsten concentration of ~1.2 ppm.

207

208 3.2. Evaluation of formation constants (β)

209 As mentioned above, the standard Gibbs free energy for H_2WO_4^0 and HWO_4^- were determined from
210 the molality of NaCl, HCl, and tungsten in each experiment using the program OptimA in the HCh
211 software package (Shvarov, 2015); the molality of HCl was calculated from the starting NaCl
212 concentration and the pH measured after each experiment. In addition to the two tungsten species, the
213 following aqueous species were also considered in the calculations: O_2 , H_2 , H^+ , OH^- , Na^+ , Cl^- , NaOH^0 ,
214 NaCl^0 , and HCl^0 . Thermodynamic data for these species were obtained from Johnson et al. (1992),
215 Shock et al. (1997), and Sverjensky et al. (1997) and values for the extended parameter for NaCl were
216 taken from Oelkers and Helgeson (1991). Thermodynamic data for the tungsten and molybdenum
217 oxide solids (WO_3 , MoO_2 and MoO_3) were taken from Pankratz and Mrazek (1982) and Robie and
218 Hemingway (1995). The sources of these data are listed in the Appendix B.

219 With the standard Gibbs free energy of HWO_4^- and H_2WO_4^0 in hand, the Gibbs free energy
220 changes for the reactions responsible for the formation of these species were calculated using the
221 standard Gibbs free energy of the other species involved in the reactions, namely WO_4^{2-} and H^+ .



224 Thermodynamic data for WO_4^{2-} and H^+ were taken from Shock et al. (1997) and Wesolowski et al.
225 (1984). The Gibbs free energy change was then converted to a formation constant ($\log \beta$) using the
226 relationship $\Delta G^\circ = -RT \ln K$. These formation constants and the uncertainty associated with their
227 determination are listed in Table 3; the uncertainty was calculated using the OptimA program. The
228 formation constants for H_2WO_4^0 and HWO_4^- at the different temperatures were fitted to the
229 Bryzgalin-Ryzhenko model (Ryzhenko et al., 1985) modified by Shvarov and Bastrakov (1999):

$$230 \log K_{(T,P)} = \frac{T_r}{T} \log K_{(T_r,P_r)} + B_{(T,P)} \left(A_{zz/a} + \frac{B_{zz/a}}{T} \right) \quad (9)$$

231 values for the parameters of which are listed in Table 4. In the equation, K is the dissociation constant of
232 the ion pair, T_r , P_r are the reference temperature and pressure, and $A_{zz/a}$ and $B_{zz/a}$ are fitting parameters.
233 The term $B_{(T,P)}$ was computed from the dissociation constant of water (Marshall and Franck, 1981) at
234 temperature T and pressure P . This fit was then used to calculate equilibrium constants ($\log K$) for the

235 tungsten oxide dissolution reactions. These values are reported in Table 5. Uncertainties in the
236 equilibrium constants were determined by calculating the log K values of each data point using the
237 tungsten activity, pH(T), and Reactions (4) and (5), and then calculating the standard deviation of these
238 values, at each temperature. The best fit points to the experimental data shown in Figures 5 to 8 were
239 calculated from these equilibrium constants.

240

241

4. DISCUSSION

4.1. Comparison to previous studies

242 Previous estimates of the thermodynamic properties of tungsten species have been based mainly on
243 the potentiometric experiments of Wesolowski et al. (1984) and the solubility experiments of Wood
244 and Vlassopoulos (1989) and Wood (1992). Wesolowski et al. (1984) showed that the tungstates,
245 HWO_4^- and WO_4^{2-} , are the dominant tungsten species in mildly to strongly saline aqueous solutions at
246 temperatures between 150 and 300 °C and near-neutral to alkaline conditions, respectively, and that
247 tungstic acid is the dominant species at low pH. Shock et al. (1997) developed a HKF model for
248 WO_4^{2-} and HWO_4^- based on the results of the experiments of Wesolowski et al. (1984), which are
249 widely used in evaluating tungsten solubility in hydrothermal fluids (Heinrich, 1990; Gibert et al.,
250 1992; Wood and Samson, 2000).

251
252 Wood and Vlassopoulos (1989) concluded that the ion pair, NaHWO_4^0 , is the dominant aqueous
253 species in solutions with high salinity based on experimental determinations of the solubility of
254 $\text{WO}_3^{\text{crystal}}$ in solutions containing up to 6 m NaCl and 1 m NaOH at 500 °C and 1 kbar. However,
255 although they concluded that H_2WO_4^0 is the dominant species at low pH, they did not consider HWO_4^-
256 in their calculation of the speciation of tungsten at higher pH and NaCl concentration. They also
257 assumed that the activity coefficients of the tungsten species were equal to unity. In order to determine
258 whether the results of their experiments could be explained without calling upon a sodium tungstate
259 species, we calculated the dissolved tungsten concentration at the conditions of their experiments
260 using the thermodynamic data from this study and that of Wood and Vlassopoulos (1989), assuming
261 that tungsten was present in their solutions only as the species H_2WO_4^0 and HWO_4^- (this study) and
262 WO_4^{2-} (Wesolowski et al., 1984). The calculated tungsten concentration is very similar to that
263 measured in the experiments of Wood and Vlassopoulos (1989) involving NaOH and NaCl, even at

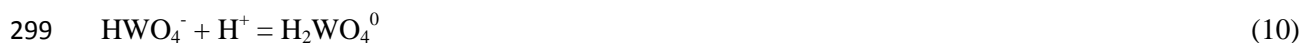
264 the highest concentrations of these solutes (Fig. 6a and 6b). This suggests strongly that HWO_4^- or
265 WO_4^{2-} and not NaHWO_4^0 were the dominant species in these experiments at mildly acidic and alkaline
266 pH, respectively. The addition of NaCl or NaOH to the solutions increases the ionic strength as well
267 as pH and, in turn, decreases the activity coefficient and increases the concentration of HWO_4^- ,
268 respectively. We note, however, that the tungsten concentrations in our acidic, lower pH experiments
269 are lower than those of Wood and Vlassopoulos (1989). We attribute this discrepancy as probably
270 being due to entrainment of solute particles during sampling in the experiments of Wood and
271 Vlassopoulos (1989). The line fit to their data by Gibert et al. (1992), suggesting higher tungsten
272 concentrations than predicted by our data, results from the higher $\log K_5$ values proposed for Reaction
273 (5).

274 As has already been mentioned, Wood (1992) determined the solubility of $\text{WO}_3^{\text{crystal}}$ in aqueous
275 solutions with variable HCl concentrations at temperatures between 300 and 600°C and 1 kbar. He
276 demonstrated that H_2WO_4^0 is the principal tungsten species at all HCl concentrations and calculated
277 $\log K$ values for the dissolution reaction (Reaction 5, this study). We extrapolated our data and those
278 of Wood (1992) using the Bryzgalin-Ryzhenko model at saturated water vapor pressure and 1kbar,
279 respectively, in order to compare the two data sets. His $\log K$ values for this reaction are 1 to 2 units
280 higher than the values determined in this study (Table 6). A possible reason for this discrepancy is that
281 he did not consider the possible formation of HWO_4^- at low HCl concentration. We cannot explain,
282 however, why the $\log K$ values reported by Wood (1992) are systematically higher than those reported
283 in this study.

284 Wood and Samson (2000) proposed that, in natural systems, tungsten is transported as the
285 species H_2WO_4^0 , HWO_4^- , WO_4^{2-} , NaHWO_4^0 , and NaWO_4^- . They calculated formation constants for
286 H_2WO_4^0 , HWO_4^- , and WO_4^{2-} based on the results of the experiments of Wood (1992) and Wesolowski
287 et al. (1984). However, in the absence of the necessary data for NaHWO_4^0 and NaWO_4^- , they assumed
288 that the formation constants for these species are equal to those for KHSO_4^0 and KSO_4^- . In order to
289 determine whether the thermodynamic data recommended by Wood and Samson (2000) are consistent
290 with our experimental data, we calculated the concentration of tungsten that we expected to observe in
291 each of our experiments, based on their data. In Figure 7, we compare the results of our experiments
292 with these predictions in plots of $\log m_{\Sigma W}$ versus $\log a_{\text{Na}^+}$ and pH (T) for 250, 300 and 350°C. As is
293 evident from this figure, the concentration of tungsten observed in our experiments is 1 to 2 log units

294 lower than that predicted from the thermodynamic data of Wood and Samson (2000) at equivalent
295 conditions.

296 For an additional comparison, we made use of the association constant reported earlier for
297 HWO_4^- (Reaction 7) and the association constant for H_2WO_4^0 calculated using the thermodynamic
298 data from for the following reaction:



$$300 \log K_{10} = \log a_{\text{H}_2\text{WO}_4^0} - \log a_{\text{HWO}_4^-} + \text{pH}$$

301 In Table 6, we compare the association constants for Reactions 7 and 10 calculated in this study with
302 those of previous studies. Our values are considerably lower than those reported previously, largely
303 because the latter were based on the data of Wood (1992), which we believe overestimated the
304 solubility of tungsten. We use these association constants in Figure 8 to predict the predominance
305 fields of H_2WO_4^0 , HWO_4^- and WO_4^{2-} . Our constants predict that H_2WO_4^0 is dominant only at pH
306 values < 2.8 , which is over one unit less than that predicted previously. The disparity is somewhat less
307 for the dominance of WO_4^{2-} , with our values predicting a predominance boundary at a pH of 5 for 200
308 °C and vapor-saturated water pressure, which is only 0.3 units less than that predicted by other studies
309 except that of Minubayeva et al. (2007), whose data are not consistent with those of other studies.

310

311 4.2. Application to natural systems

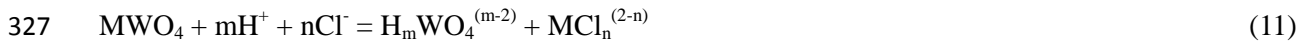
312 Tungsten is deposited as the minerals scheelite (CaWO_4) and wolframite ($(\text{Fe,Mn})\text{WO}_4$) in
313 ore-forming hydrothermal systems. Here we make use of the results of our experimental study to
314 quantitatively evaluate the conditions under which tungsten transport is optimized and those that
315 promote the deposition of scheelite and wolframite. For simplicity, we represent wolframite by its
316 endmember, ferberite (FeWO_4). Thermodynamic data for the minerals were taken from Holland and
317 Powell (1998), Wood and Samson (2000) and Robie and Hemingway (1995), and for aqueous species
318 other than the tungsten species from Johnson et al. (1992), Shock et al. (1997), Sverjensky et al. (1997)
319 and Tagirov et al. (1997). This information is detailed in Appendix B.

320

321 4.2.1. Chloride ion concentration

322 Although we have shown that ion pairs involving Na^+ and complexes involving Cl^- do not contribute
323 to tungsten solubility in hydrothermal fluids, chloride is important for the transport of both Ca^{2+} and

324 Fe^{2+} , which participate in the formation of scheelite and ferberite, respectively. In fact, Wood and
325 Samson (2000) proposed that high chloride activity in the fluid facilitates the dissolution of tungsten
326 species via the reaction:



328 $\text{M} = \text{Ca}^{2+}$ or Fe^{2+} ; $m = 0$ to 2 ; $n = 0$ to 2 or 4

329

330 4.2.2. Temperature

331 In order to evaluate the effect of cooling on the precipitation of tungsten minerals, we modeled the
332 concentration of tungsten as a function of temperature at conditions of scheelite or ferberite saturation.
333 The results of this modeling show that scheelite and ferberite both precipitate from the solution with
334 decreasing temperature (Fig 9a and 9b). However, only a small amount of scheelite precipitated from
335 the scheelite-saturated solution, and the tungsten concentration of the solution did not decrease
336 appreciably from its initial concentration. In contrast, almost all the tungsten in the ferberite-saturated
337 solution precipitated (as ferberite). This difference in behavior indicates a stronger dependence of the
338 solubility of ferberite on temperature than that of scheelite.

339

340 4.2.3. pH

341 As shown by the results of this experimental study, the solubility of the WO_3 and the nature of the
342 dominant aqueous tungsten species are strongly affected by pH. However, the manner in which pH
343 affects the solubility of the tungsten minerals in natural systems is unclear. We also note that the pH of
344 ore-forming fluid is commonly controlled by fluid-rock interaction. To this end, we modeled the
345 solubility of scheelite and ferberite in a brine as a function of pH (Fig 10a and 10b), and evaluated the
346 effect of fluid-rock interaction on pH and on the solubility of tungsten in an ore-forming fluid (Fig
347 10c and 10d). The results of this modeling show that scheelite and ferberite dissolve in acidic and
348 alkaline solutions, but deposit from solutions with near neutral pH. In the strongly acidic solutions,
349 scheelite and ferberite dissolved via Reaction (11), whereas in the alkaline solutions, they dissolved
350 through Reactions (12) and (13). The effect of the fluid-rock interaction was to drive the pH of the
351 acidic and alkaline solutions to a value of ~ 5 , which induced tungsten mineral precipitation.



354

355 4.2.4. Calcium and iron concentration

356 Several studies have proposed that fluid mixing is important for tungsten ore-formation as this process
357 introduces Ca^{2+} and Fe^{2+} into the hydrothermal ore fluid, which commonly has very low
358 concentrations of these cations because of its exsolution from a highly fractionated S-type granitic
359 magma (Lecumberri-Sanchez et al., 2017; Yang et al., 2019). To test the fluid-mixing hypothesis, we
360 modeled the mixing of a high salinity, tungsten-saturated brine, containing no Ca^{2+} and Fe^{2+} , with a
361 low salinity, tungsten-free fluid containing Ca^{2+} or Fe^{2+} at 400 °C and 1000 bar (Fig 11a and 11b). The
362 former brine represents the hydrothermal fluid originating from the granitic magma, and the latter
363 brine a formational water. The results of the modeling show that scheelite and ferberite precipitate
364 strongly in response to increased concentrations of calcium and iron via Reaction (14).



366 $\text{M} = \text{Fe}^{2+}$ or Ca^{2+} ; $m = 0$ or 1 or 2 ; $n = 0$ to 2 or 4

367 In short, a hot, very acidic or alkaline saline hydrothermal fluid with low concentrations of Ca and Fe
368 has a high capacity to transport tungsten. Tungsten mineral precipitation, on the other hand is favored
369 by low temperature, near neutral pH and high concentrations of Ca and Fe.

370

371

5. CONCLUSIONS

372 The results of this study show that tungsten is dissolved in NaCl-bearing fluids as H_2WO_4^0 at low pH
373 and HWO_4^- at moderately acidic to near-neutral pH. Contrary to the conclusion of some earlier studies,
374 NaHWO_4^0 and NaWO_4^- do not play a role in tungsten transport. The distribution of tungsten species is
375 therefore controlled mainly by pH, and salinity promotes dissolution of tungsten minerals by
376 increasing the ionic strength of the solution. The geological modeling in this paper suggests that a hot,
377 saline, acidic or alkaline hydrothermal fluid with low concentrations of calcium and iron is an ideal
378 ore-fluid for tungsten.

379

380

ACKNOWLEDGEMENTS

381 The experimental work in this paper was carried out in the Fluid-Rock Interaction Laboratory,
382 Department of Earth and Planetary Sciences, McGill University and was funded by the Strategic
383 Priority Research Program (B) of the Chinese Academy of Sciences (XDB18000000); a NSERC

384 Discovery grant to AEW-J; the National Natural Science Foundation of China (41603052; 41673067);
385 the National Key Research and Development Program of China (2016YFC0600204); and a Chinese
386 Government Scholarship from the China Scholarship Council. We thank Anna Katharina Jung for her
387 assistance in conducting the ICP-MS analyses, and Caroline Seyler for her assistance in conducting
388 the XRD analyses. Discussions with Olga Vasyukova, Yuan Mei, Jethro Sanz-Robinson, and Jiaxin
389 Wang helped improve the manuscript. We are grateful for the constructive reviews of George Dan
390 Miron, Joel Brugger, and an anonymous referee that improved this manuscript significantly, and the
391 editorial assistance and comments of Editor Zoltan Zajacz and Jeffrey G. Catalano.

392

393

REFERENCES

- 394 Bailly L., Grancea L. and Kouzmanov K., (2002) Infrared microthermometry and chemistry of wolframite from
395 the Baia Sprie epithermal deposit, Romania. *Econ. Geol.* **97**, 415–423.
- 396 Campbell A., Rye D. and Petersen U. (1984) A hydrogen and oxygen isotope study of the San Cristobal Mine,
397 peru - implications of the role of water to rock ratio for the genesis of wolframite deposits. *Econ. Geol.*
398 **79**, 1818–1832.
- 399 Campbell A.R. and Robinsoncook S. (1987) Infrared fluid inclusion microthermometry on coexisting
400 wolframite and quartz. *Econ. Geol.* **82**, 1640–1645.
- 401 Gibert F., Moine B., Schott J. and Dandurand J.L. (1992) Modeling of the transport and deposition of tungsten
402 in the scheelite-bearing calc-silicate gneisses of the montagne noire, France. *Contrib. Mineral. Petrol.*
403 **112**, 371–384.
- 404 Heinrich C.A. (1990) The chemistry of hydrothermal tin(-tungsten) ore deposition. *Econ. Geol.* **85**, 457–481.
- 405 Helgeson H.C., Kirkham D.H. and Flowers, G.C. (1981) Theoretical prediction of the thermodynamic behavior
406 of aqueous electrolytes by high pressures and temperatures; IV, Calculation of activity coefficients,
407 osmotic coefficients, and apparent molal and standard and relative partial molal properties to 600
408 degrees C and 5kb. *Am. J. Sci.* **281**, 1249–1516.
- 409 Holland, T.J.B. and Powell, R. (1998) An internally consistent thermodynamic data set for phases of petrological
410 interest. *J. Metamorph. Geol.* **16**, 309–343.
- 411 Johnson J.W., Oelkers E.H. and Helgeson H.C. (1992) SUPCRT92: A software package for calculating the
412 standard molal thermodynamic properties of minerals, gases, aqueous species, and reactions from 1 to
413 5000 bar and 0 to 1000°C. *Comput. and Geosci.* **18**, 899–947.
- 414 Keppler H. and Wyllie P.J. (1991) Partitioning of Cu, Sn, Mo, W, U, and Th between melt and aqueous fluid in
415 the systems haplogranite-H₂O–HCl and haplogranite-H₂O–HF. *Contrib. Mineral. Petrol.* **109**,
416 139–150.
- 417 Kestin J., Sengers J.V., Kamgar-Parsi, B. and Sengers, J.M.H.L. (1984) Thermophysical Properties of Fluid
418 H₂O. *J. Phys. Chem. Ref. Data* **13**, 175–183.
- 419 Korges M., Weis P., Lüders V. and Laurent O. (2018). Depressurization and boiling of a single magmatic fluid as
420 a mechanism for tin-tungsten deposit formation. *Geology* **46**, 75–78.
- 421 Lecumberri-Sanchez P., Vieira R., Heinrich C.A., Pinto F. and Walle M. (2017) Fluid-rock interaction is decisive
422 for the formation of tungsten deposits. *Geology* **45**, 579–582.

- 423 Lu H.Z., Liu Y.M., Wang C.L., Xu Y.Z. and Li H.Q. (2003) Mineralization and fluid inclusion study of the
424 Shizhuyuan W-Sn-Bi-Mo-F skarn deposit, Hunan province, China. *Econ. Geol.* **98**, 955–974.
- 425 Manning D.A.C. and Henderson P. (1984) The behavior of tungsten in granitic melt-vapor systems. *Contrib.*
426 *Mineral. Petrol.* **86**, 286–293.
- 427 Marshall W.L. and Franck E.U. (1981) Ion product of water substance, 0–1000 °C, 1–10,000 bars New
428 International Formulation and its background. *J. Phys. Chem. Ref. Data* **10**, 295–304.
- 429 Mei, Y., Sherman, D., Liu, W. and Brugger, J. (2014) Metal complexation and ion hydration in low density
430 hydrothermal fluids: ab initio molecular dynamics simulation of Cu(I) and Au(I) in chloride solutions
431 (25-1000 °C, 1-5000 bar). *Geochim. Cosmochim. Acta* **131**, 196-212.
- 432 Mei, Y., Sherman, D., Liu, W., Etschmann, B., Testemale, D. and Brugger, J. (2015) Zinc complexation in
433 chloride-rich hydrothermal fluids (25 to 600 °C): a thermodynamic model derived from ab initio
434 molecular dynamics. *Geochim. Cosmochim. Acta* **150**, 265-284.
- 435 Migdisov A.A. and Williams-Jones A.E. (2007) An experimental study of the solubility and speciation of neodymium (III) fluoride in F-bearing
436 aqueous solutions. *Geochim. Cosmochim. Acta* **71**, 3056–3069.
- 437 Minubaeva Z. (2007). UV spectroscopic studies of the hydrothermal geochemistry of molybdenum and tungsten.
438 ETH Zurich.
- 439 Ni P., Wang X.-D., Wang G.-G., Huang J.-B., Pan J.-Y. and Wang, T.-G. (2015) An infrared microthermometric
440 study of fluid inclusions in coexisting quartz and wolframite from Late Mesozoic tungsten deposits in
441 the Gannan metallogenic belt, South China. *Ore Geol. Rev.* **65**, 1062–1077.
- 442 Oelkers E.H. and Helgeson H.C. (1990) Triple-ion anions and polynuclear complexing in supercritical
443 electrolyte solutions. *Geochim. Cosmochim. Acta* **54**, 727–738.
- 444 Oelkers E.H. and Helgeson H.C. (1991). Calculation of activity coefficients and degrees of formation of neutral
445 ion pairs in supercritical electrolyte solutions. *Geochim. Cosmochim. Acta* **55**, 1235–1251.
- 446 Pankratz L. and Mrazek R.V. (1982) Thermodynamic properties of elements and oxides. U.S. *Bureau of Mines*
447 *Bulletin*, 672.
- 448 Polya D.A. (1988) Efficiency of hydrothermal ore formation and the Panasqueira W–Cu(Ag)–Sn vein deposit.
449 *Nature* **333**, 838.
- 450 Polya D.A. (1989) Chemistry of the main-stage ore-forming fluids of the Panasqueira W-Cu(Ag)-Sn deposit,
451 Portugal - Implications for models of ore genesis. *Econ. Geol.* **84**, 1134–1152.
- 452 Robie R.A. and Hemingway B.S. (1995) Thermodynamic properties of minerals and related substances at
453 298.15 K and 1 bar (10⁵ pascals) pressure and at higher temperatures.
- 454 Romer R.L. and Lüders V. (2006) Direct dating of hydrothermal W mineralization: U–Pb age for hübnerite
455 (MnWO₄), Sweet Home Mine, Colorado. *Geochim. Cosmochim. Acta* **70**, 4725–4733.
- 456 Ryzhenko B.N., Bryzgalin O.V., Artamkina I.Y., Spasennykh M.Y. and Shapkin A.I. (1985) An electrostatic
457 model for the electrolytic dissociation of inorganic substances dissolved in water. *Geochem. Int.* **22**,
458 128–144.
- 459 Shock E.L., Sassani D.C., Willis M. and Sverjensky D.A. (1997) Inorganic species in geologic fluids:
460 Correlations among standard molal thermodynamic properties of aqueous ions and hydroxide
461 complexes. *Geochim. Cosmochim. Acta* **61**, 907–950.
- 462 Shvarov Y. (2015) A suite of programs, OptimA, OptimB, OptimC, and OptimS compatible with the Unitherm
463 database, for deriving the thermodynamic properties of aqueous species from solubility, potentiometry
464 and spectroscopy measurements. *Appl. Geochem.* **55**, 17–27.
- 465 Shvarov Y.V. and Bastrakov E. (1999) HCh: a software package for geochemical equilibrium modelling. User's
466 Guide 25.

- 467 Shvarov Y.V. (2008). HCh: New potentialities for the thermodynamic simulation of geochemical systems
468 offered by windows. *Geochem. Int.* **46**, 834–839.
- 469 Sverjensky D.A., Shock E.L. and Helgeson H.C. (1997) Prediction of the thermodynamic properties of aqueous
470 metal complexes to 1000°C and 5 kb. *Geochim. Cosmochim. Acta* **61**, 1359–1412.
- 471 Soloviev S.G. and Kryazhev S.G. (2017) Geology, mineralization, and fluid inclusion characteristics of the
472 Skrytoe reduced-type W skarn and stockwork deposit, Sikhote-Alin, Russia. *Miner. Depos.* **52**,
473 903–928.
- 474 Tagirov, B.R., Zotov, A.V., and Akinfiev, N.N. (1997) Experimental study of dissociation of HCl from 350 to
475 500°C and from 500 to 2500 bars: Thermodynamic properties of HCl°(aq). *Geochim. Cosmochim. Acta*
476 **61**, 4267-4280.
- 477 Testemale, D., Brugger, J., Liu, W., Etschmann, B. and Hazemann, J.-L. (2009) In-situ X-ray absorption study of
478 Iron(II) speciation in brines up to supercritical conditions. *Chem. Geol.* **264**, 295-310.
- 479 Timofeev A., Migdisov A.A. and Williams-Jones A.E. (2017) An experimental study of the solubility and
480 speciation of tantalum in fluoride-bearing aqueous solutions at elevated temperature. *Geochim.*
481 *Cosmochim. Acta* **197**, 294–304.
- 482 Wei W., Hu R., Bi X., Peng J., Su W., Song S. and Shi S. (2012) Infrared microthermometric and stable isotopic
483 study of fluid inclusions in wolframite at the Xihuashan tungsten deposit, Jiangxi province, China.
484 *Miner. Depos.* **47**, 589–605.
- 485 Wesolowski D., Drummond S.E., Mesmer R.E. and Ohmoto H. (1984). Hydrolysis equilibria of tungsten(VI) in
486 aqueous sodium-chloride solutions to 300-degrees-c. *Inorg. Chem.* **23**, 1120–1132.
- 487 Wood S.A. (1992). Experimental determination of the solubility of WO₃(s) and the thermodynamic properties of
488 H₂WO₄(aq) in the range 300–600 C at 1 kbar: calculation of scheelite solubility. *Geochim. Cosmochim.*
489 *Acta* **56**, 1827–1836.
- 490 Wood S.A. and Samson I.M. (2000). The Hydrothermal Geochemistry of Tungsten in Granitoid Environments: I.
491 Relative Solubilities of Ferberite and Scheelite as a Function of T, P, pH, and *m*_{NaCl}. *Econ. Geol.* **95**,
492 143–182.
- 493 Wood S.A. and Vlassopoulos D. (1989). Experimental determination of the hydrothermal solubility and
494 speciation of tungsten at 500° C and 1 kbar1, 2. *Geochim. Cosmochim. Acta* **53**, 303–312.
- 495 Yang, J.-H., Zhang, Z., Peng, J.-T., Liu, L. and Leng, C.-B. (2019) Metal source and wolframite precipitation
496 process at the Xihuashan tungsten deposit, South China: Insights from mineralogy, fluid inclusion and
497 stable isotope. *Ore Geol. Rev.* **111**, 102965.
- 498 Zhu Y.-N. and Peng J.-T. (2015). Infrared microthermometric and noble gas isotope study of fluid inclusions in
499 ore minerals at the Woxi orogenic Au–Sb–W deposit, western Hunan, South China. *Ore Geol. Rev.* **65**,
500 Part 1, 55–69.

501

502

503 **Figures Legends**

504

505 Figure 1. A schematic diagram showing the experimental set-up employed in this study. Malleable carbon rings
506 provided an airtight seal upon closure of the autoclave.

507

508 Figure 2. A diagram showing the results of experiments of variable duration conducted at 250 °C (kinetic

509 experiments) with an aqueous solution containing 1 mol/kg NaCl and 0.01 mol/kg HCl. From the diagram, it is
510 evident that the solubility of $\text{WO}_3^{\text{crystal}}$ reached a steady state concentration after six days.

511

512 Figure 3. Results of experiments at 350 °C, 300 °C, 250 °C. (a), (c), and (e) showing the concentrations of
513 dissolved tungsten ($\log m\Sigma W$) as a function of the activity of Na^+ ($\log a\text{Na}^+$) and (b), (d) and (f) the tungsten
514 concentrations as a function of pH. The filled blue circles in (a), (c), (e) represent the results of experiments
515 designed to determine the dependence of the solubility of WO_3 on Na^+ activity at a $\text{pH}_{(25\text{ }^\circ\text{C})}$ of ~ 2 . The results of
516 experiments designed to determine the dependence of WO_3 solubility on pH (at nearly constant $\log a\text{Na}^+$) are
517 illustrated in (d), (e), and (f); the data for these experiments are also shown in (a), (c), (e) using the symbols
518 employed in (d), (e), and (f). The equations “ $y = ax - b$ ” represent linear regressions of the data.

519

520 Figure 4. A plot showing values of $\log a\Sigma W$ at 350, 300, 250 °C as a function of pH, assuming that the
521 solubility of $\text{WO}_3^{\text{crystal}}$ can be fully explained by its dissolution as H_2WO_4^0 and HWO_4^- . The $\log a\Sigma W$ values
522 were adjusted to $\text{pH}(T) = 1.8$ (350 °C), and $\text{pH}(T) = 1.4$ (300 and 250 °C) on the basis of the stoichiometry of
523 Reactions 4 and 5. The $\log a\Sigma W$ values at 350 °C prior to the adjustment are shown for comparison. The
524 dashed lines with arrowheads indicate the trends of tungsten activity from low to high sodium ion activity.

525

526 Figure 5. Plots of $\log a\Sigma W$ and $\log a\text{HWO}_4^-$ versus $\text{pH}(T)$ at 350 °C (a, b), 300 °C (c, d), and 250 °C (e, f).
527 The filled blue circles in (a), (c), (e) represent the results of the experiments at the temperature of interest, the
528 orange curves show the fits to the data based on the $\log K$ values for Reactions 4 and 5 and the yellow and blue
529 dashed lines indicate the activity of HWO_4^- and H_2WO_4^0 based on the $\log K$ values for Reaction 4 and 5,
530 respectively. The parameters $a\Sigma W$, $a\text{HWO}_4^-$, and $\text{pH}(T)$ refer to the total tungsten activity, the activity of
531 HWO_4^- , and the pH of the experimental solution at each temperature, respectively. The dotted lines represent the
532 best fits to the data for $a\text{HWO}_4^-$ versus $\text{pH}(T)$ at the different temperatures and “ $y = ax - b$ ” the equations of
533 these lines. Diagrams (a), (c) and (e) illustrate the independence of tungsten activity from pH at low pH values
534 due to the dissolution of $\text{WO}_3^{\text{crystal}}$ as H_2WO_4^0 , and its dependence on pH at high pH values because of the
535 formation of HWO_4^- .

536

537 Figure 6. (a) A comparison of the fit to the data for $\log m\Sigma W$ as a function of $\log m\text{NaOH}$ reported in this study to
538 those for the data of Wood and Vlassopoulos (1989; 500 °C and 1000 bar) and those of Wood and Vlassopoulos

539 (1989) recalculated by Gibert et al. (1992). (b) A comparison of the fit to the data for log $m\Sigma W$ as a function of log
540 $mNaCl$ reported in this study to those for the data of Wood and Vlassopoulos (1989) and those of Wood and
541 Vlassopoulos (1989) recalculated by Gibert et al. (1992). The tungsten species used in the calculation were
542 $H_2WO_4^0$, HWO_4^- , and WO_4^{2-} . See text for further detail.

543
544 Figure 7. Plots of log $a\Sigma W$ versus log aNa^+ and log $a\Sigma W$ versus pH comparing the results of the experiments
545 conducted in this study with the expected log $a\Sigma W$ values of these experiments calculated using log K values
546 reported by Wood and Samson (2000) based on the results of the experiments of Wood (1992) for 350 °C (a),
547 300 °C (c), 250 °C (e, f) and water saturated vapor pressure.

548
549 Figure 8. Predominance fields for $H_2WO_4^0$, HWO_4^- , and WO_4^{2-} in aqueous liquid as a function of temperature
550 and pH at saturated vapor pressure a) and 1000 bar b) based on the results of this study; thermodynamic data for
551 WO_4^{2-} were taken from Shock (1992). Also shown are the predominance fields for these species based on the
552 experimental data of Wesolowski et al. (1984), Wood and Samson (2000), and Minubaeva (2007).

553
554 Figure 9. Plots showing the concentrations of aqueous species and tungsten mineral solubility as a function of
555 temperature. The fluid contained 1.5 m NaCl, 0.02 m HCl, at 400 °C, 1000 bar, and a pH of 3.05 and was
556 saturated with respect to scheelite (a) and ferberite (b).

557
558 Figure 10. (a) and (b). Plots showing the concentration of aqueous species and tungsten mineral solubility as a
559 function of increasing pH. The fluid contained 1.5 m NaCl and 0.02 m HCl, at 400 °C, 1000 bar and an initial
560 pH of 3.05, and was saturated with respect to scheelite and ferberite. It was titrated with NaOH to produce the
561 pH increase. (c) A plot showing the total tungsten concentration, pH and tungsten mineral solubility resulting
562 from progressive interaction of the fluid with microcline. The fluid contained 1.5 m NaCl and 0.02 m HCl, at
563 400 °C, 1000 bar and an initial pH of 3.05, was saturated with respect to scheelite and ferberite, and was
564 buffered to a final pH of ~5. (d). A plot showing the total tungsten concentration, pH and tungsten mineral
565 solubility resulting from progressive interaction of the fluid with a greisen (quartz-muscovite-paragonite). The
566 fluid contained 1.5 m NaCl, 0.1 m NaOH, at 400 °C, 1000 bar and an initial pH of 9.15, was saturated with
567 respect to scheelite and ferberite, and was buffered to a final pH of ~5. The Rock/fluid ratio in (c) and (d)

568 represents the mass of minerals over the mass of fluid.

569

570 Figure 11. Plots showing the effect on tungsten concentration and tungsten mineral solubility of mixing an ore

571 fluid containing 4 m NaCl, 0.0003 m HCl and 80 ppm tungsten at 400 °C, 1000 bar, and a pH of 4.64 with a

572 fluid at the same temperature and pressure containing 0.6m NaCl, 0.0001 m HCl and 0.001 m CaCl₂ (a) and

573 0.6m NaCl, 0.0001 m HCl and 0.001 m 0.001 m FeCl₂ (b). The mixing ratio represents the mass of the second

574 fluid over that of the ore fluid.

Table 1. Values for thermodynamic parameters from Helgeson and Kirkham (1974) used in the activity coefficient function (Equation 1).

T (°C)	A		B		$b_{\gamma, \text{NaCl}}$	
	Sat.	1000 bar	Sat.	1000 bar	Sat.	1000 bar
200	0.7994	0.7195	0.3639	0.3591	0.0485	0.0647
250	0.9593	0.8221	0.3766	0.3690	0.0203	0.0485
300	1.2175	0.9502	0.3925	0.3792	-0.0244	0.0278
350	1.8234	1.1178	0.418	0.3902	-0.1076	0.0024
400		1.3502		0.4024		-0.0292

Table 2. Compositions of quenched experimental solutions from experiments. The values of a_{Na^+} (T) and pH (T) are calculated at interested temperatures.

T (°C)	NaCl(m)	HCl(m), 10^{-3}	W(m), 10^{-6}	pH(25 °C)	a_{Na^+} (T)	pH (T)
350	1.40	5.59	611	2.48	0.10	3.65
350	1.40	6.49	452	2.42	0.10	3.60
350	1.40	11.4	337	2.17	0.10	3.37
350	1.40	19.2	201	1.95	0.10	3.15
350	1.40	30.8	180	1.74	0.10	2.95
350	1.40	50.7	96.0	1.52	0.10	2.73
350	1.25	6.68	432	2.40	0.10	3.56
350	1.00	6.63	349	2.39	0.09	3.52
350	0.85	8.51	230	2.28	0.08	3.39
350	0.70	7.65	270	2.32	0.07	3.39
350	0.70	10.7	218	2.17	0.07	3.25
350	0.70	19.8	137	1.91	0.07	2.99
350	0.70	27.8	84.2	1.76	0.07	2.84
350	0.70	42.3	69.9	1.58	0.07	2.66
350	0.70	70.5	55.0	1.36	0.07	2.44
350	0.40	9.35	106	2.21	0.05	3.19
350	0.40	10.9	143	2.14	0.05	3.12
350	0.40	9.27	152	2.21	0.05	3.19
350	0.30	13.7	78.6	2.03	0.05	2.96
350	0.30	8.65	94.9	2.23	0.05	3.16
350	0.20	13.2	67.6	2.03	0.04	2.89
350	0.10	11.5	72.6	2.06	0.02	2.81
350	0.10	11.2	62.6	2.07	0.02	2.82
350	0.085	11.9	37.7	2.04	0.02	2.77
350	0.07	10.6	28.9	2.08	0.02	2.78
350	0.05	8.21	41.0	2.18	0.02	2.82
350	0.02	8.06	25.8	2.17	0.01	2.67
350	0.01	6.30	33.6	2.26	0.005	2.67
350	0.01	11.4	40.0	2.01	0.005	2.45
350	0.01	16.0	39.2	1.87	0.004	2.33
350	0.01	28.5	33.1	1.63	0.004	2.14
350	0.01	32.6	30.6	1.57	0.004	2.10
350	0.01	42.5	30.1	1.46	0.004	2.02

350	0.01	56.7	32.6	1.35	0.003	1.94
350	0.01	71.3	34.3	1.26	0.003	1.87
350	0.0005	11.5	27.5	1.99	0.0003	2.32
350	0.0005	9.20	27.5	2.08	0.0003	2.39
300	3.00	5.07	188	2.55	0.37	3.31
300	3.00	5.15	174	2.55	0.37	3.30
300	3.00	5.13	148	2.55	0.37	3.31
300	2.00	6.53	81.3	2.43	0.30	3.12
300	2.00	7.49	79.3	2.37	0.30	3.06
300	2.00	6.82	87.4	2.41	0.30	3.10
300	1.40	1.82	396	2.97	0.24	3.55
300	1.40	2.77	251	2.79	0.24	3.40
300	1.40	4.22	162	2.60	0.24	3.23
300	1.40	7.63	119	2.35	0.24	2.98
300	1.40	13.6	46.4	2.11	0.24	2.74
300	1.40	21.7	46.6	1.89	0.24	2.53
300	1.40	24.1	29.3	1.85	0.24	2.49
300	1.00	9.76	52.1	2.23	0.20	2.81
300	0.90	10.5	64.9	2.19	0.19	2.76
300	0.80	10.9	44.1	2.02	0.17	2.72
300	0.70	9.73	47.2	2.21	0.16	2.74
300	0.70	11.5	39.7	2.14	0.16	2.67
300	0.70	9.05	59.5	2.25	0.16	2.78
300	0.40	9.39	37.8	2.21	0.11	2.66
300	0.30	10.4	25.7	2.15	0.09	2.56
300	0.25	10.3	22.1	2.15	0.08	2.54
300	0.20	9.62	28.7	2.17	0.07	2.53
300	0.10	8.29	16.3	2.20	0.04	2.49
300	0.085	10.6	19.1	2.09	0.04	2.37
300	0.07	10.4	16.7	2.14	0.03	2.35
300	0.04	9.48	23.9	2.11	0.02	2.32
300	0.01	1.79	24.3	2.80	0.01	2.90
300	0.01	16.6	14.5	1.85	0.01	2.01
300	0.01	17.8	9.84	1.82	0.01	1.98
300	0.01	25.4	13.0	1.67	0.01	1.85
300	0.01	27.2	17.7	1.65	0.01	1.83
300	0.01	28.1	7.34	1.63	0.01	1.82
300	0.01	37.3	16.7	1.52	0.01	1.72
300	0.01	43.6	7.10	1.45	0.01	1.67
300	0.01	58.4	20.6	1.34	0.01	1.57
300	0.01	71.0	22.4	1.26	0.005	1.51
300	0.01	75.1	10.1	1.23	0.005	1.49
300	0.01	75.5	17.5	1.23	0.005	1.49
300	0.01	78.0	9.16	1.22	0.005	1.48
300	0.01	101	21.7	1.12	0.005	1.40
300	0.005	11.5	12.1	2.00	0.003	2.12
300	0.005	9.77	10.4	2.06	0.004	2.18

250	4.00	2.56	67.8	2.86	0.74	3.31
250	4.00	2.96	67.8	2.80	0.74	3.25
250	3.00	5.00	40.4	2.56	0.62	2.98
250	2.00	7.27	23.2	2.38	0.48	2.75
250	1.40	5.53	31.3	2.49	0.38	2.82
250	1.40	8.65	18.1	2.29	0.38	2.63
250	1.40	14.1	14.0	2.08	0.38	2.42
250	1.40	19.7	10.2	1.93	0.38	2.27
250	1.40	31.7	5.92	1.73	0.38	2.07
250	1.00	9.78	11.6	2.23	0.30	2.53
250	0.70	11.5	11.1	2.14	0.24	2.41
250	0.40	12.3	8.31	2.09	0.16	2.31
250	0.30	12.8	12.1	2.06	0.13	2.26
250	0.25	11.3	11.5	2.11	0.11	2.29
250	0.20	12.8	10.1	2.04	0.09	2.22
250	0.01	24.7	5.44	1.69	0.007	1.77
250	0.01	28.1	3.02	1.63	0.007	1.72
250	0.01	37.5	6.92	1.51	0.007	1.61
250	0.01	38.0	8.92	1.51	0.007	1.60
250	0.01	44.8	6.51	1.44	0.006	1.54
250	0.01	59.5	6.97	1.33	0.006	1.44
250	0.01	60.3	4.99	1.32	0.006	1.44
250	0.01	60.5	8.06	1.32	0.006	1.43
250	0.01	73.6	10.1	1.24	0.006	1.36
250	0.01	74.8	3.83	1.24	0.006	1.36
250	0.0005	2.75	12.5	2.59	0.0004	2.61
250	0.0005	1.77	17.5	2.77	0.0005	2.79
250	0.0005	7.63	6.52	2.16	0.0004	2.20

Table 3. Formation constants ($\log\beta$) for the tungsten species identified in this study based on experiments between 250 to 350 °C.

	250 °C	300 °C	350 °C
$\text{WO}_4^{2-} + 2\text{H}^+ = \text{H}_2\text{WO}_4^0$	8.23 ± 0.01	9.20 ± 0.01	10.96 ± 0.01
$\text{WO}_4^{2-} + \text{H}^+ = \text{HWO}_4^-$	5.58 ± 0.02	6.51 ± 0.01	7.99 ± 0.01

Table 4. Bryzgalin-Ryzhenko parameters derived for tungsten species based on the formation constants determined in this study.

	pK (298)	A (zz/a)	B (zz/a)
H_2WO_4^0	6.570	1.412	0.000
HWO_4^-	3.413	1.150	0.000

Table 5. Logarithms of equilibrium constants (logK) and their associated uncertainty for the WO₃ dissolution reactions

	250 °C	300 °C	350 °C
$\text{WO}_3^{\text{cryst}} + \text{H}_2\text{O} = \text{H}_2\text{WO}_4^0$	-5.26 ± 0.26	-4.98 ± 0.25	-4.62 ± 0.10
$\text{WO}_3^{\text{cryst}} + \text{H}_2\text{O} = \text{HWO}_4^- + \text{H}^+$	-7.89 ± 0.30	-7.69 ± 0.29	-7.58 ± 0.18

Table 6. Association constants and solubility products for tungsten species derived from this and previous studies.

Association constants (logK)												
	T °C	200	250	300	350	400	500	600	P bars	Method	Reference	
logK ₁₀	HWO ₄ ⁻ + H ⁺ = H ₂ WO ₄ ⁰	2.63 ^d	2.63	2.71	2.96				Sat.	MBR model	<i>This study</i>	
		4.20	4.10	3.90	3.90				Sat.	Calculation ^a	Heinrich (1990)	
				4.30					Sat.	Calculation ^b	Gibert et al. (1992)	
		3.85	3.68	3.70	4.25				Sat.	MBR model extrapolation ^c	Wood and Samson (2000)	
		3.56		3.39		3.96			500	HKF model extrapolation ^e	Wood and Samson (2000)	
							5.50		1000	Calculation ^b	Gibert et al. (1992)	
		3.37		3.08		3.14	3.57	4.16	1000	HKF model extrapolation ^e	Wood and Samson (2000)	
		2.52	2.48	2.48	2.51	2.59	2.88	3.31	1000	MBR model extrapolation ^d	<i>This study</i>	
logK ₇	WO ₄ ²⁻ + H ⁺ = HWO ₄ ⁻	4.96 ^d	5.60	6.47	8.00				Sat.	MBR model	<i>This study</i>	
		5.34	6.07	6.89					Sat.	Potentiometric measurement	Wesolowski et al. (1984)	
		6.31	6.79						Sat.	Uv-vis spectroscopy	Minubayeva (2007)	
		5.40	6.10	6.90	7.70				Sat.	Calculation ^a	Heinrich (1990)	
				6.90						Calculation ^b	Gibert et al. (1992)	
		5.29	6.00	6.85	8.04				Sat.	HKF model extrapolation ^e	Shock et al. (1997)	
		5.15		6.48		8.10			500	HKF model extrapolation ^e	Wood and Samson (2000)	
							8.10			Calculation ^b	Gibert et al. (1992)	
		5.03		6.23		7.58	9.17	11.10	1000	HKF model extrapolation ^e	Wood and Samson (2000)	
		5.02	5.61	6.23	6.88	7.58	9.17	11.09	1000	HKF model extrapolation ^e	Shock et al. (1997)	
4.47	4.93	5.44	6.03	6.73	8.63	10.98	1000	MBR model extrapolation ^d	<i>This study</i>			
Solubility constants (pK = -logK)												
	T °C	200	250	300	350	400	500	600	P bars	Method	References	
pK ₅	WO ₃ ^{cryst} + H ₂ O = H ₂ WO ₄ ⁰		5.26	4.98	4.62				Sat.	Solubility experiment	<i>This study</i>	
			3.81	3.61	3.29				Sat.	MBR model extrapolation ^c	Wood and Samson (2000)	
							2.55			1000	Solubility experiment	Wood and Vlassopoulos (1989)
					4.00		3.40	3.10	2.70	1000	Solubility experiment	Wood (1992)
								2.55		1000	Calculation ^b	Gibert et al. (1992)
		5.77	5.42	5.17	4.97	4.80	4.50	4.60	1000	MBR model extrapolation ^d	<i>This study</i>	

pK ₄	$\text{WO}_3^{\text{cryst}} + \text{H}_2\text{O} = \text{HWO}_4^- + \text{H}^+$	7.89	7.69	7.58				Sat.	Solubility experiment	<i>This study</i>	
		7.50	7.31	7.54				Sat.	HKF model extrapolation ^e	Shock et al. (1997)	
		7.73	7.22	6.86	6.63	6.54	6.83	7.81	1000	HKF model extrapolation ^e	Shock et al. (1997)
		8.29	7.90	7.65	7.49	7.39	7.38	7.92	1000	MBR model extrapolation ^d	<i>This study</i>

Note: ^a Calculated from Wesolowski et al. (1984).

^b Calculated from Wesolowski et al. (1984) and Wood and Vlassopoulos (1989).

^c Calculated from MBR (Bryzgalin-Ryzhenko Model) parameters based on the data of Wood and Samson (2000).

^d Calculated from MBR (Bryzgalin-Ryzhenko Model) parameters based on data from this study.

^e Calculated from HKF (Helgeson-Kirkham-Flowers Model) parameters.

Figure 1

Wang, X.-S., Timofeev, A., Williams-Jones, A.E., Shang, L.-B., Bi, X.-W., 2019.

[Click here to download high resolution image](#)

An experimental study of the solubility and speciation of tungsten in NaCl-bearing aqueous solutions at 250, 300, and 350 °C. *Geochimica et Cosmochimica Acta*, 265: 313-329.

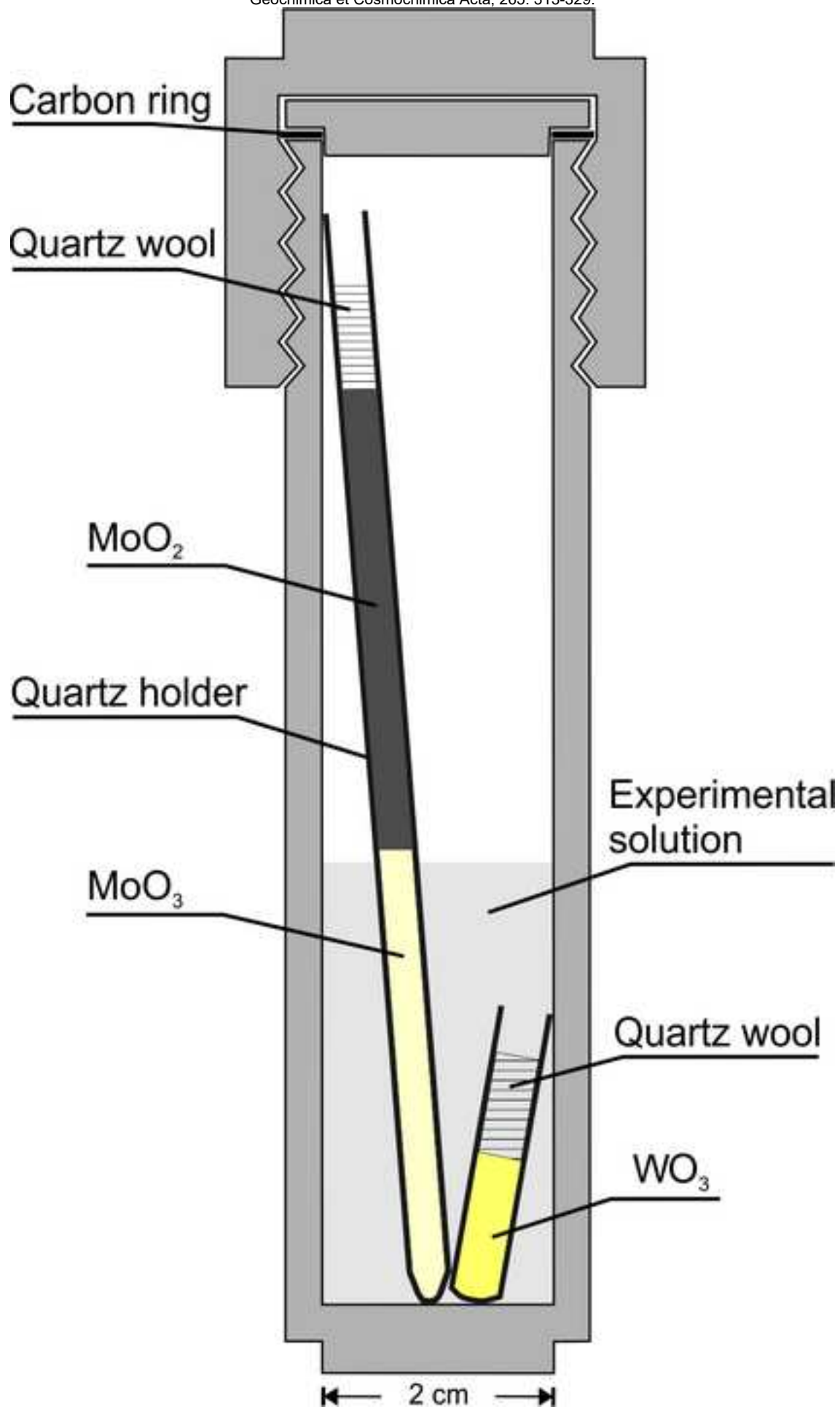


Figure 2

[Click here to download high resolution image](#)

Wang, X.-S., Timofeev, A., Williams-Jones, A.E., Shang, L.-B., Bi, X.-W., 2019.

An experimental study of the solubility and speciation of tungsten in NaCl-bearing aqueous solutions at 250, 300, and 350 °C.

Geochimica et Cosmochimica Acta, 265: 313-329.

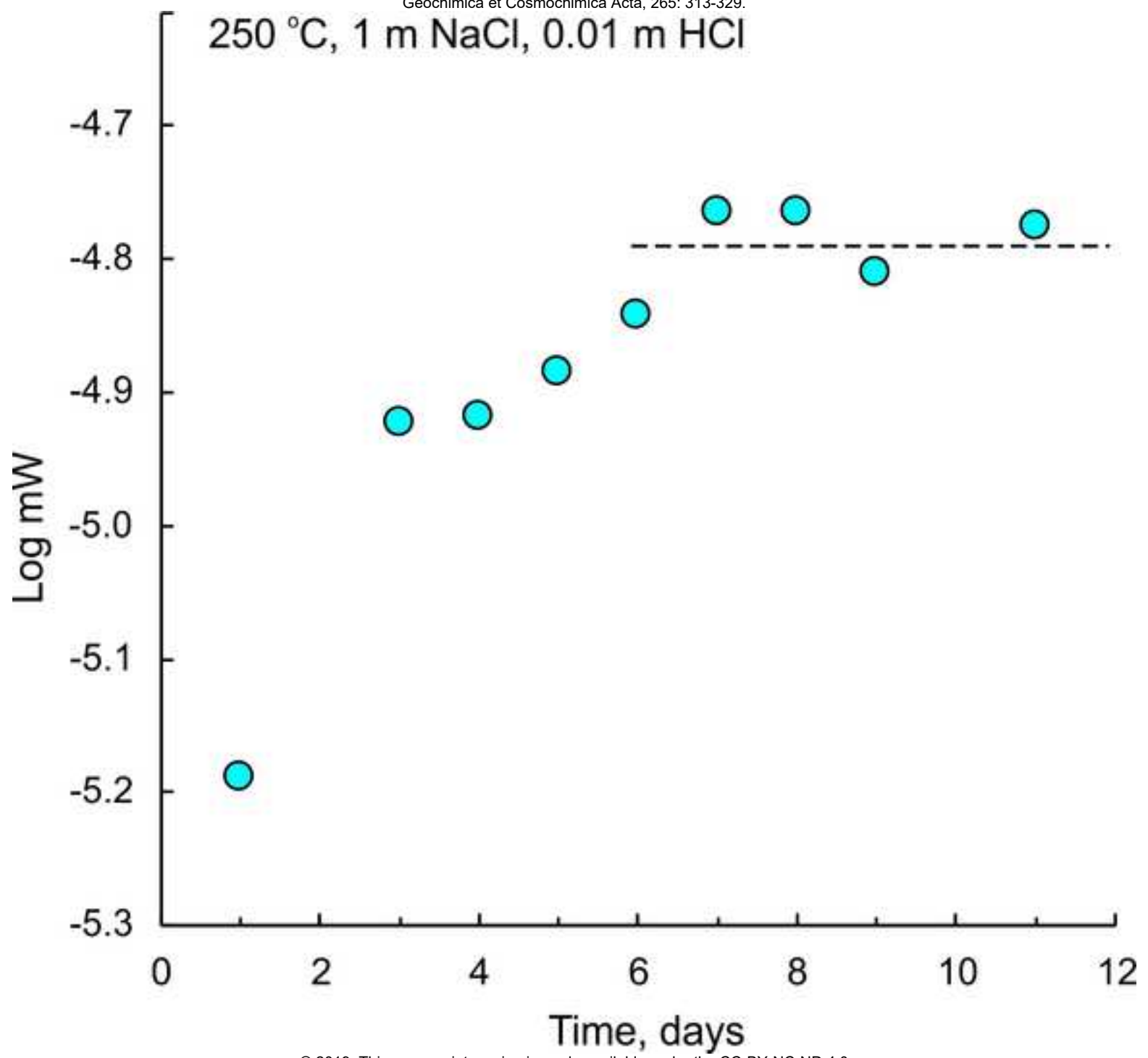


Figure 3

Wang, X.-S., Timofeev, A., Williams-Jones, A.E., Shang, L.-B., Bi, X.-W., 2019. An experimental study of the solubility and speciation of tungsten in NaCl-bearing aqueous solutions at 250, 300, and 350 °C. *Geochimica et Cosmochimica Acta*, 265: 313-329.

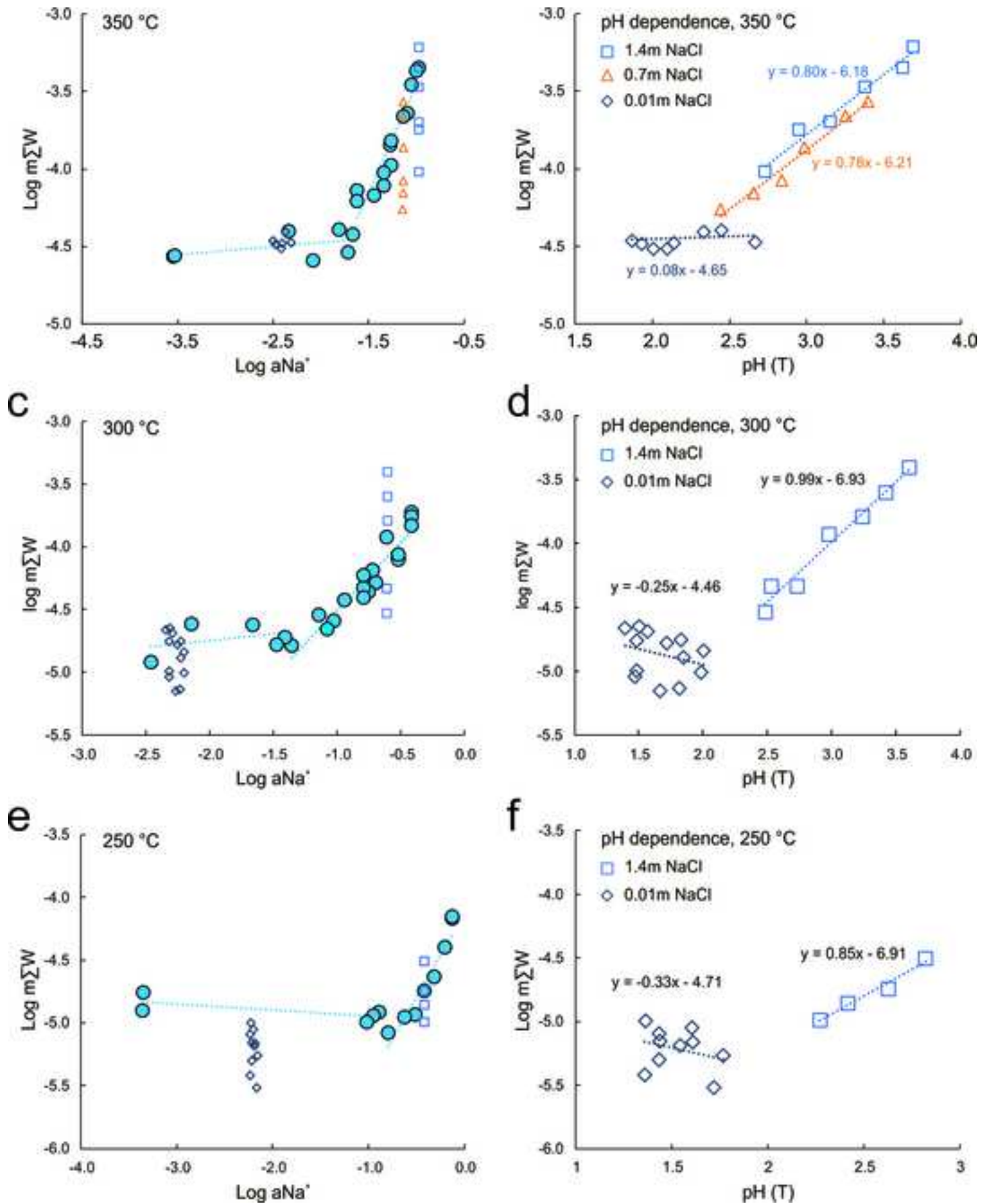


Figure 4

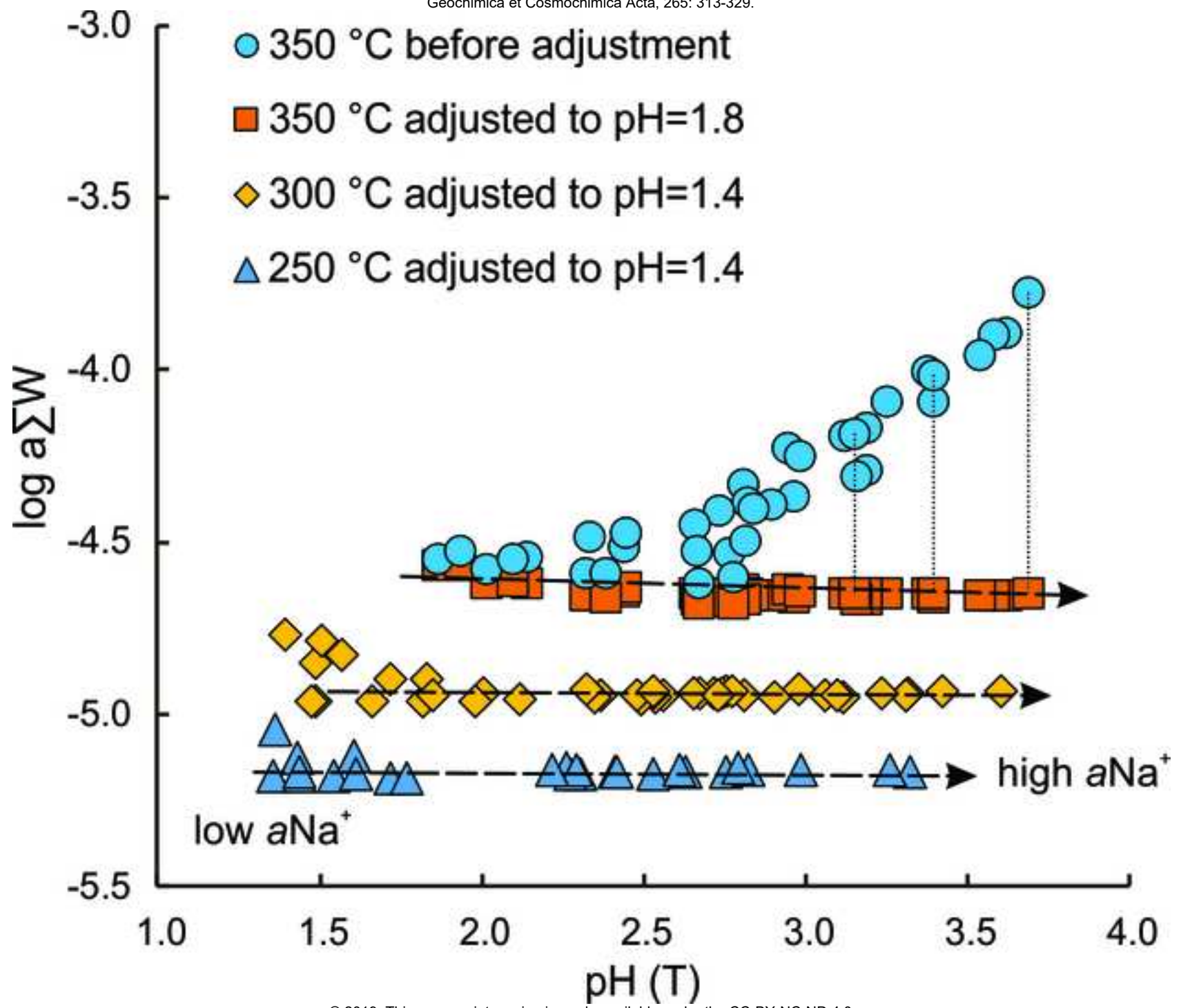


Figure 5

Wang, X.-S., Timofeev, A., Williams-Jones, A.E., Shang, L.-B., Bi, X.-W., 2019. An experimental study of the solubility and speciation of tungsten in NaCl-bearing aqueous solutions at 250, 300, and 350 °C. *Geochimica et Cosmochimica Acta*, 265: 313-329.

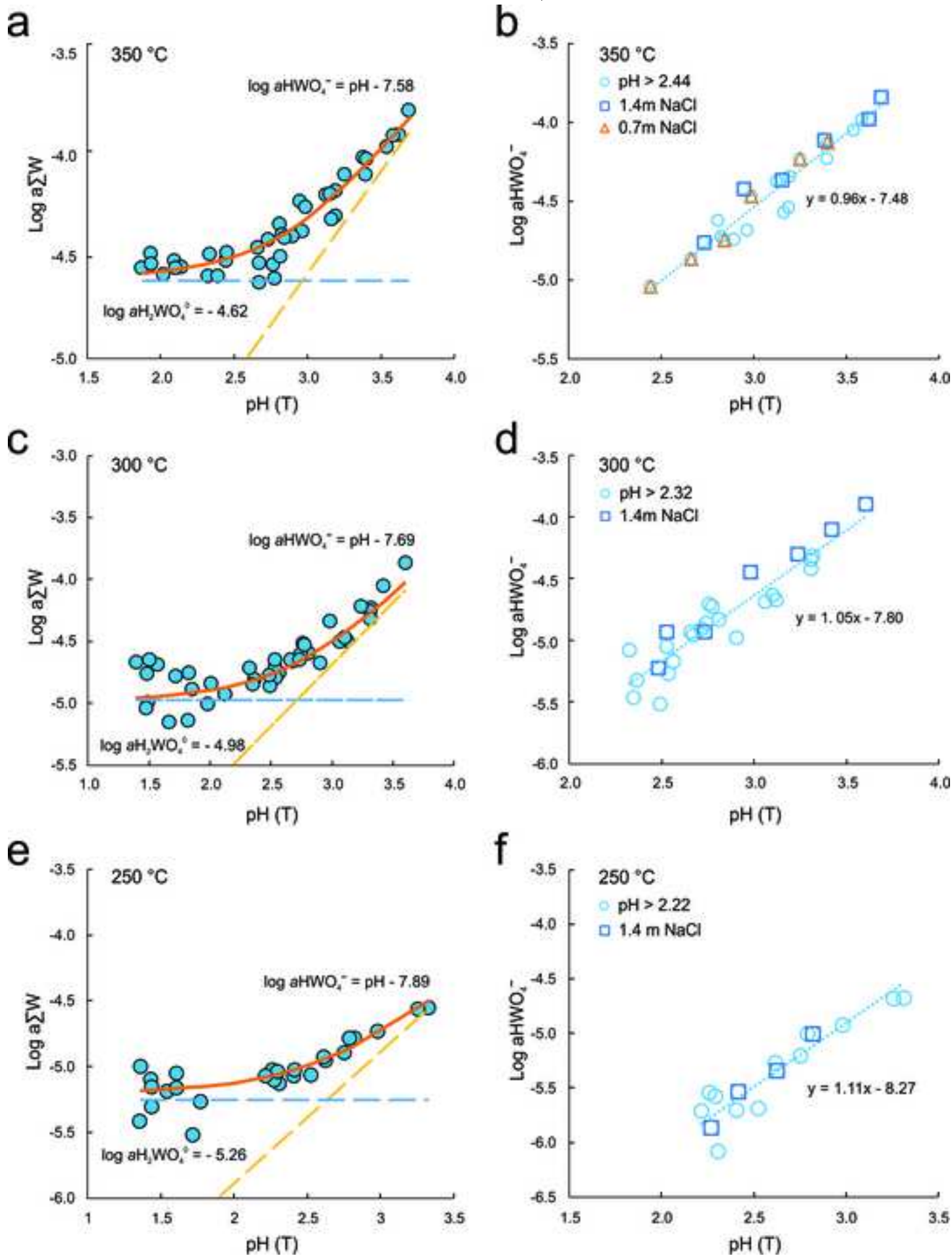


Figure 6

[Click here to download high resolution image](#)

Wang, X.-S., Timofeev, A., Williams-Jones, A.E., Shang, L.-B., Bi, X.-W., 2019.

An experimental study of the solubility and speciation of tungsten in NaCl-bearing aqueous solutions at 250, 300, and 350 °C. *Geochimica et Cosmochimica Acta*, 265: 313-329.

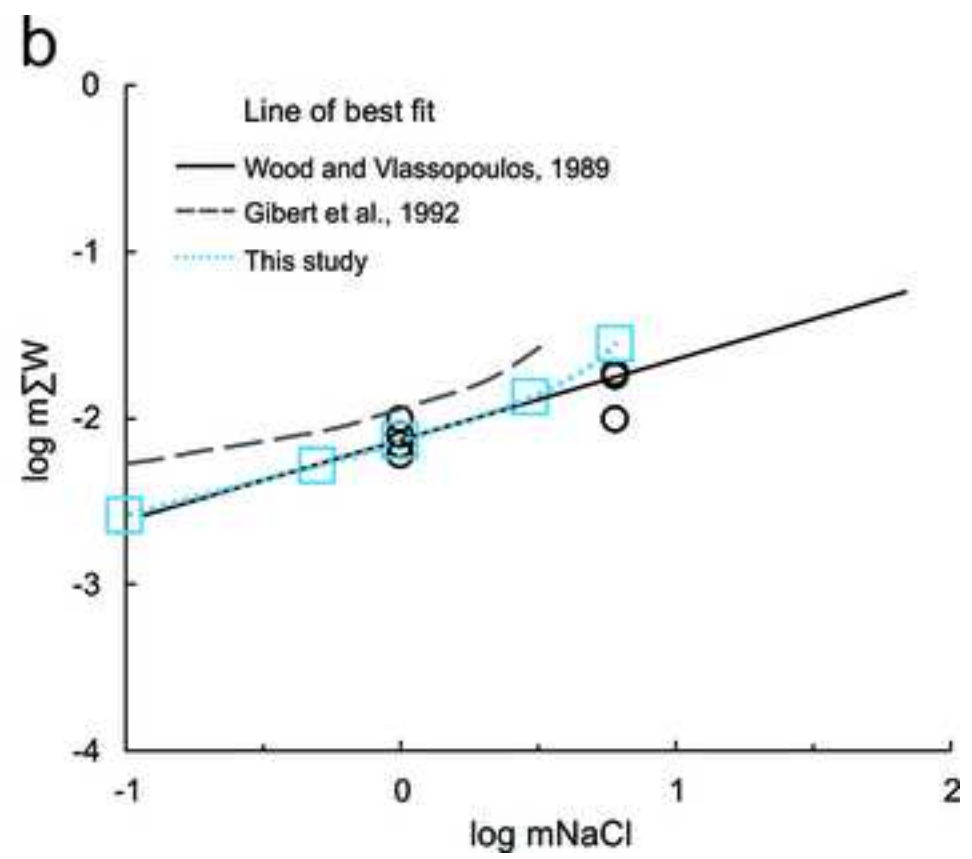
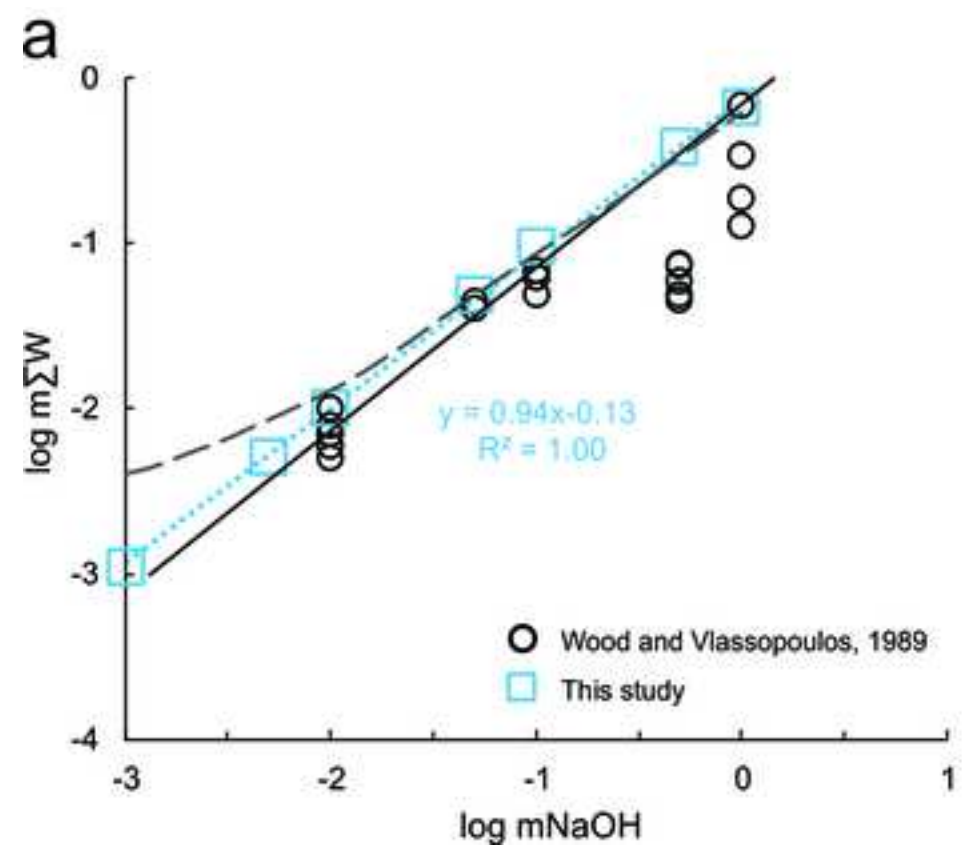


Figure 7

Wang, X.-S., Timofeev, A., Williams-Jones, A.E., Shang, L.-B., Bi, X.-W., 2019.

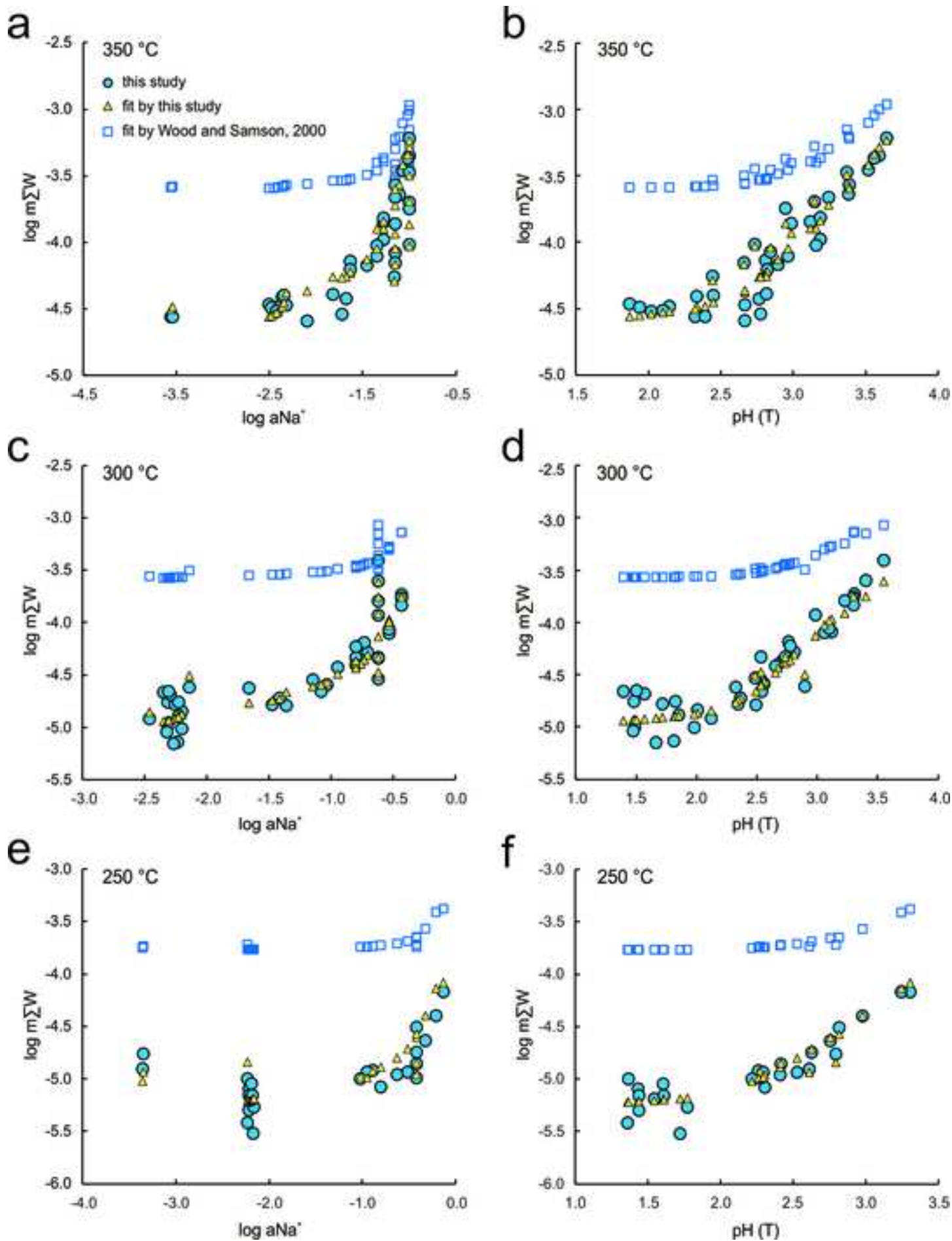
An experimental study of the solubility and speciation of tungsten in NaCl-bearing aqueous solutions at 250, 300, and 350 °C. *Geochimica et Cosmochimica Acta*, 265: 313-329.

Figure 8

Wang, X.-S., Timofeev, A., Williams-Jones, A.E., Shang, L.-B., Bi, X.-W., 2019.

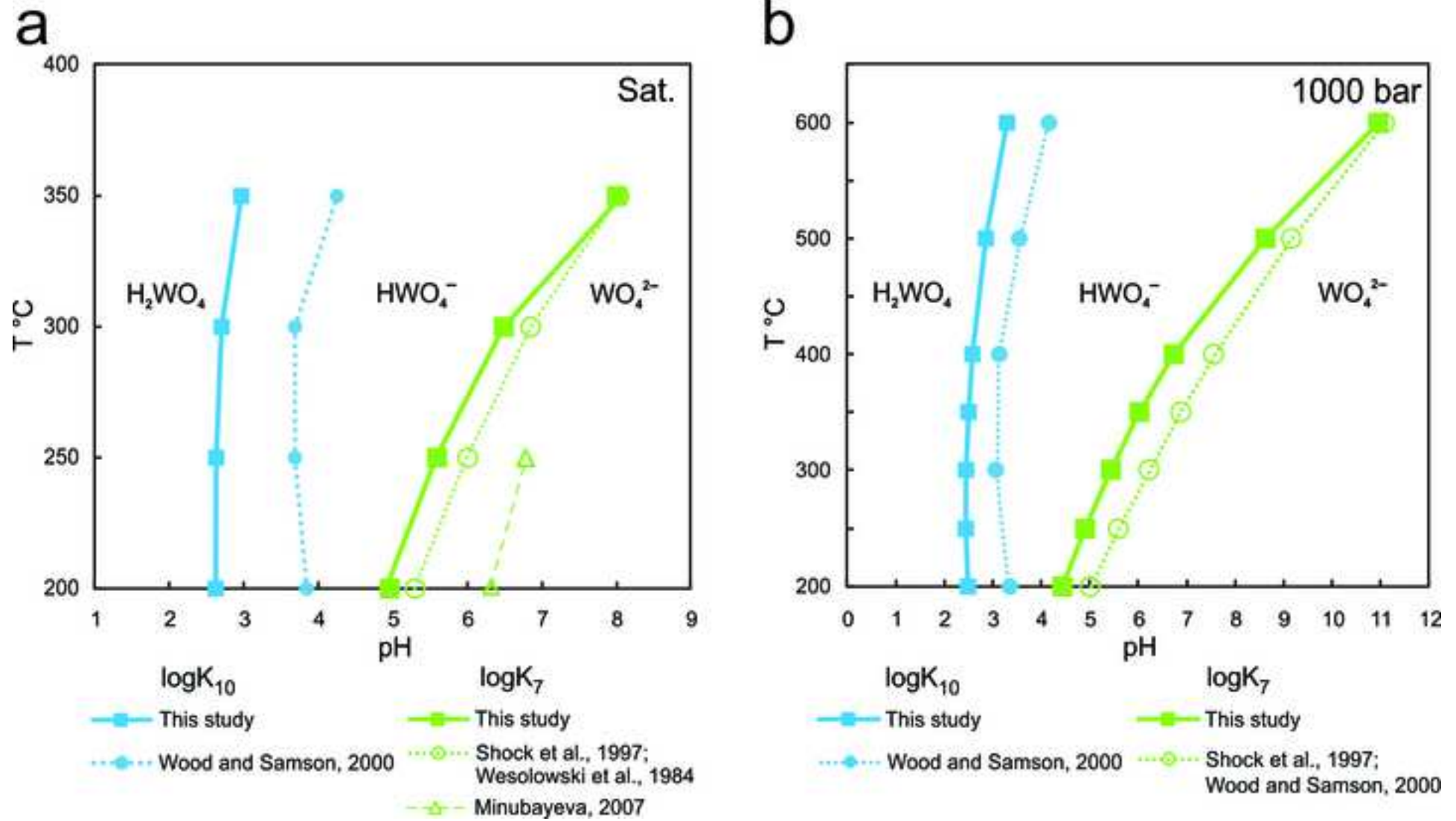
[Click here to download high resolution image](#)An experimental study of the solubility and speciation of tungsten in NaCl-bearing aqueous solutions at 250, 300, and 350 °C. *Geochimica et Cosmochimica Acta*, 265: 313-329.

Figure 9

Wang, X.-S., Timofeev, A., Williams-Jones, A.E., Shang, L.-B., Bi, X.-W., 2019.

[Click here to download high resolution image](#)

An experimental study of the solubility and speciation of tungsten in NaCl-bearing aqueous solutions at 250, 300, and 350 °C. *Geochimica et Cosmochimica Acta*, 265: 313-329.

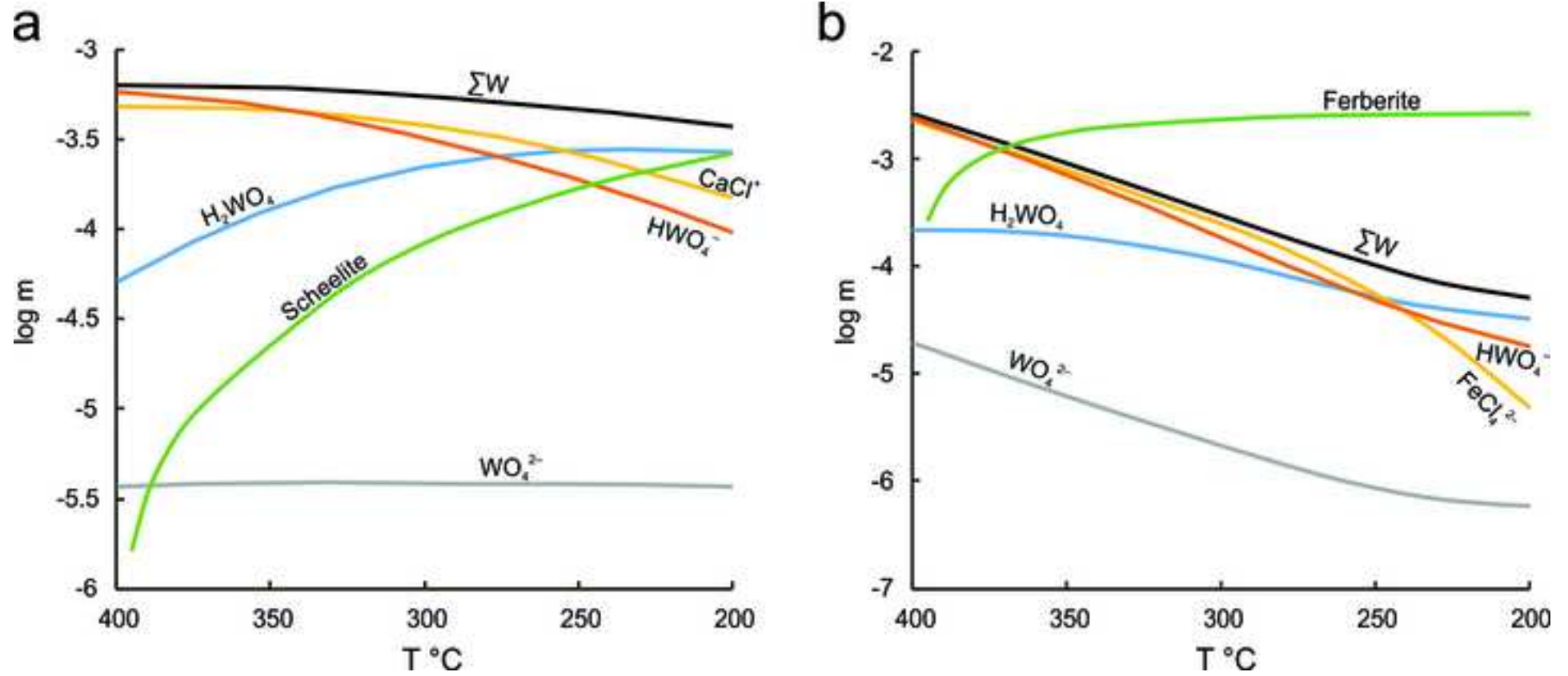


Figure 10[Click here to download high resolution image](#)

Wang, X.-S., Timofeev, A., Williams-Jones, A.E., Shang, L.-B., Bi, X.-W., 2019.

An experimental study of the solubility and speciation of tungsten in NaCl-bearing aqueous solutions at 250, 300, and 350 °C.

Geochimica et Cosmochimica Acta, 265: 313-329.

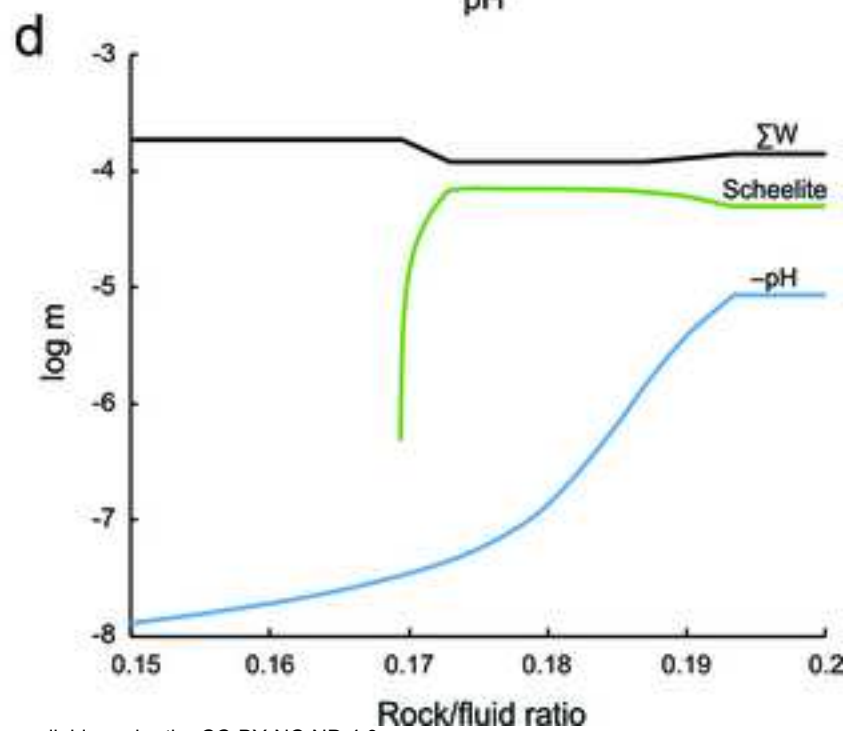
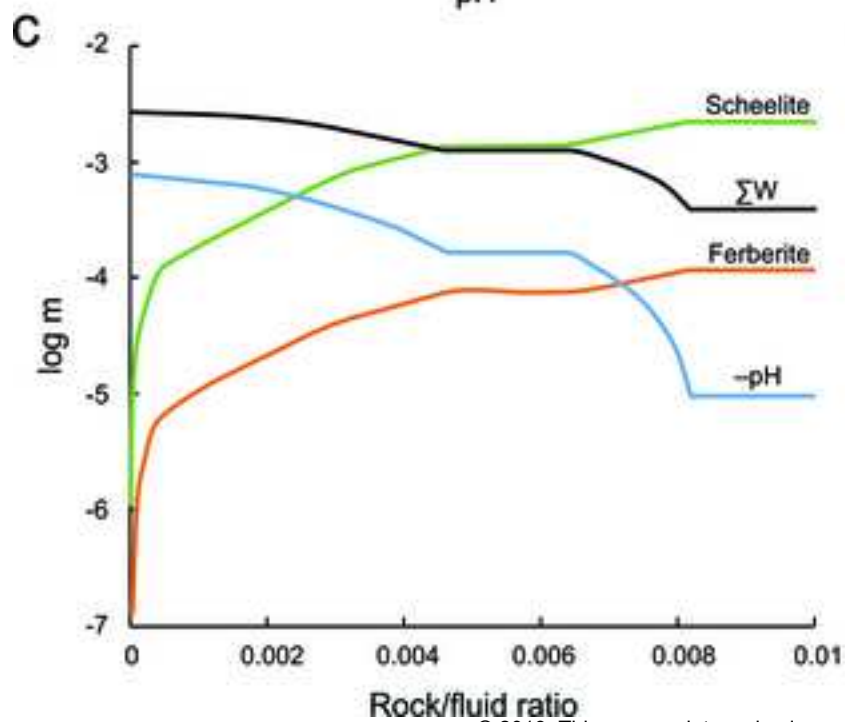
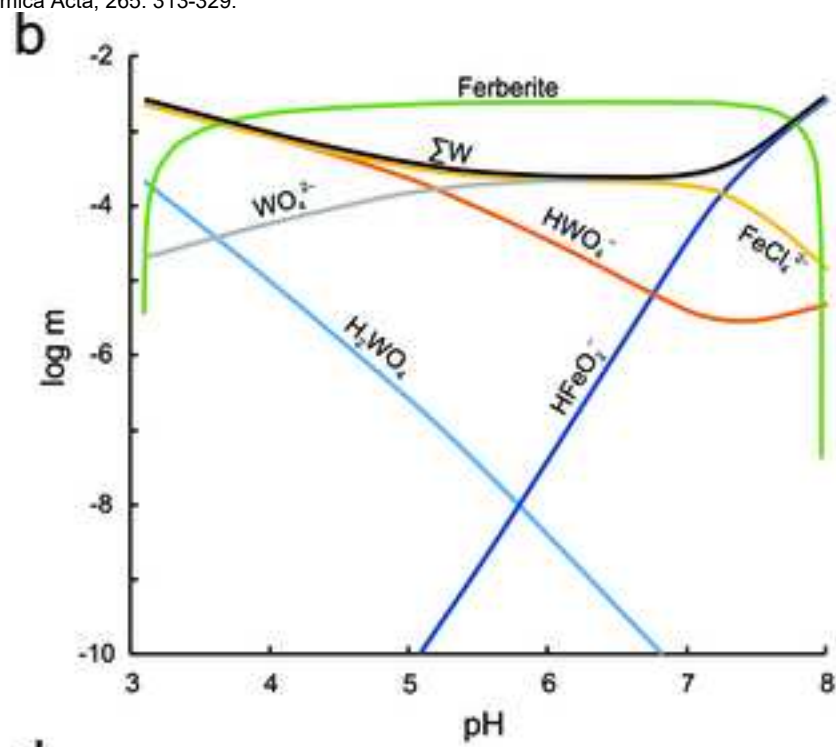
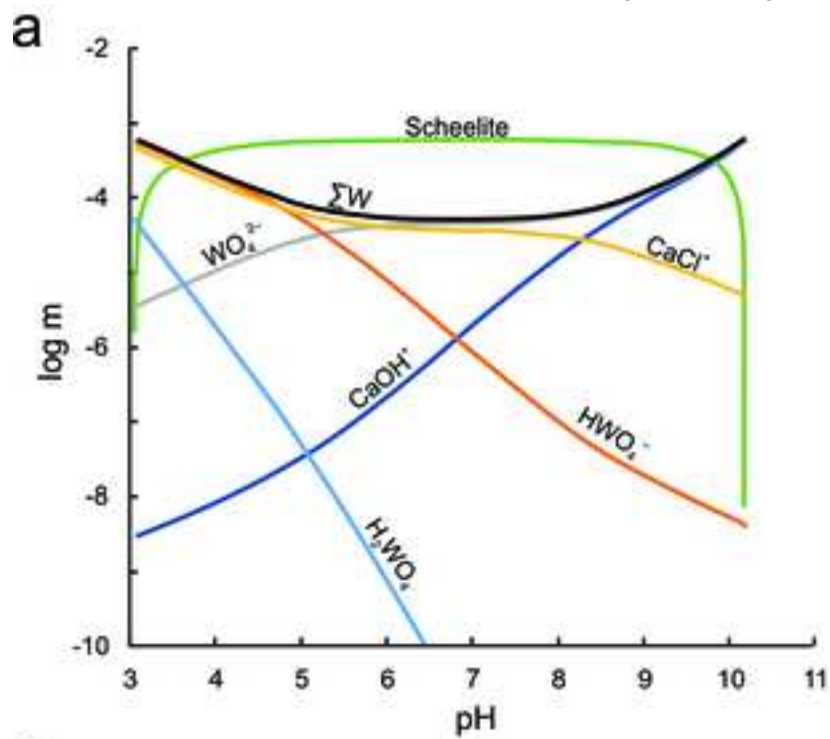
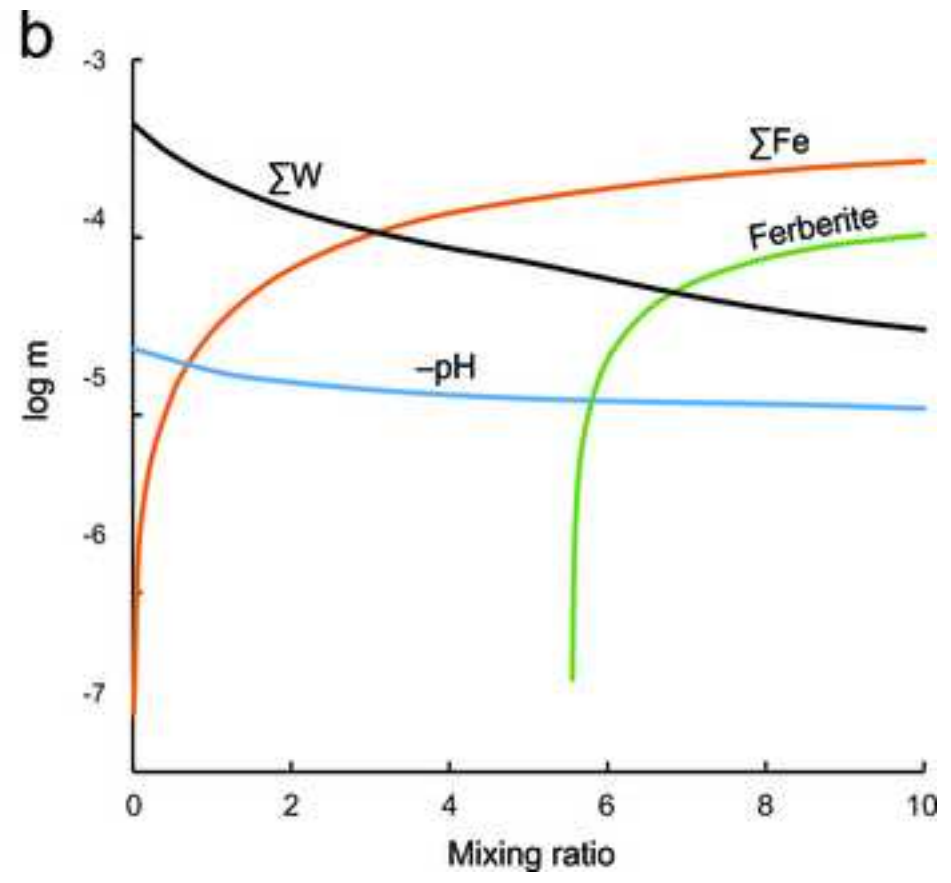
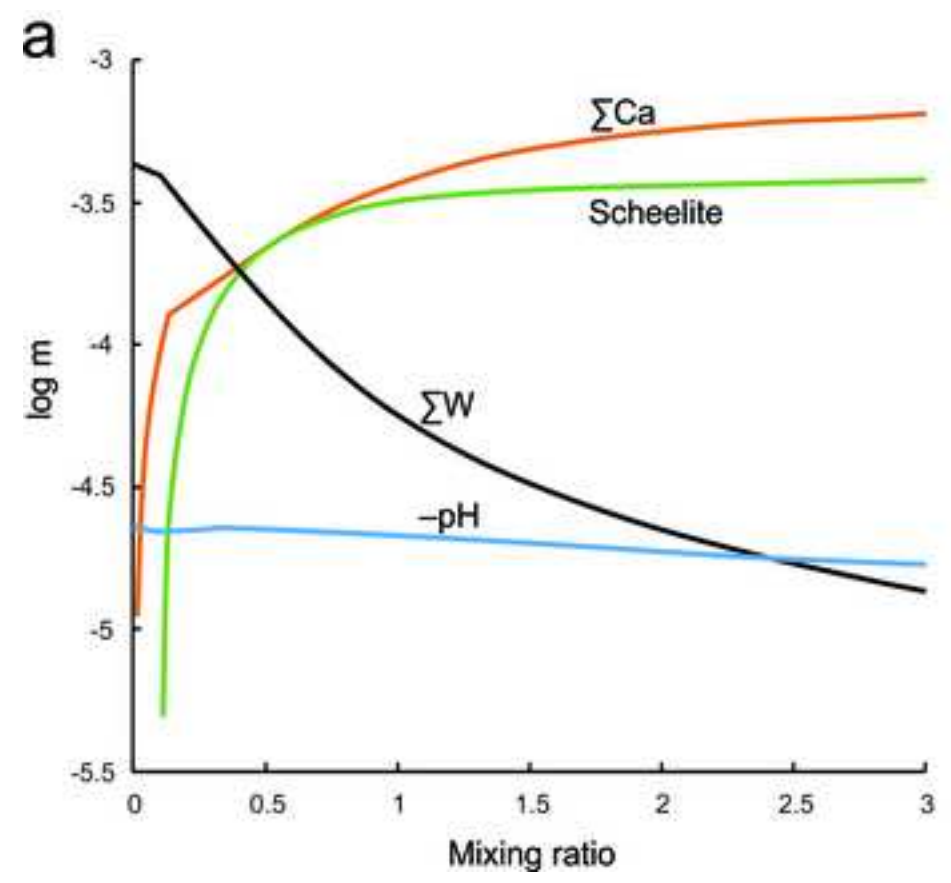


Figure 11

[Click here to download high resolution image](#)

Wang, X.-S., Timofeev, A., Williams-Jones, A.E., Shang, L.-B., Bi, X.-W., 2019.

An experimental study of the solubility and speciation of tungsten in NaCl-bearing aqueous solutions at 250, 300, and 350 °C. *Geochimica et Cosmochimica Acta*, 265: 313-329.



Appendix A and B

[Click here to download Appendix A and B.docx](#)

Wang, X.-S., Timofeev, A., Williams-Jones, A.E., Shang, L.-B., Bi, X.-W., 2019.

An experimental study of the solubility and speciation of tungsten in NaCl-bearing aqueous solutions at 250, 300, and 350 °C. *Geochimica et Cosmochimica Acta*, 265: 313-329.